Response to Reviewer #1

Reviewer #1 Comments and Suggestions for Authors:
The paper 'Tropospheric bromine monoxide in Ny-Ålesund: source analysis and impacts on atmospheric chemistry' by Li et al. provides an extended study on the relationship between enhanced BrO levels, ozone depletion events and influencing meteorological factors. The core data set consists of time series (2017 – 2023) of BrO and aerosol amounts derived from MAX-DOAS measurements. In addition, many other data sets including in situ measurements, satellite observations, trajectory analyses and model results are used to explore the conditions which favor the formation and recycling of enhanced BrO levels. One important conclusion from the study is that sea ice is the dominant bromine source. The data set is unique, and many of the conclusions are important and relevant. Nevertheless, the study lacks some scientific rigor and clear conclusions.

Author's Response: We thank Reviewer #1 for the valuable comments, which greatly improve this manuscript. Please kindly find our point-by-point responses to the problems/comments below in blue, and changes to the manuscript in orange.

Major comments:

Q1.1: The overall conclusions of the paper are rather weak and vague, especially with respect to the number and extent of the used data sets. As an example, the last sentence of the abstract states:" These results provide long-term observational evidence linking BrO to sea-ice and SSA processes, advancing understanding of Arctic bromine activation and its implications for springtime ozone depletion." In essence, this statement says nothing. The authors should be more specific about their findings.

A1.1: We have revised the abstract and summary.

The corresponding abstract section of the manuscript has been modified as below:

"Arctic tropospheric bromine monoxide (BrO) plays a critical role in atmospheric chemistry, particularly during springtime ozone depletion events. While sources such as sea ice, open ocean, aerosols, and snowpack have been proposed, their relative contributions remain uncertain. In this study, we addressed this uncertainty using long-term Multi-Axis Differential Optical Absorption Spectroscopy observations of BrO and aerosol profiles in Ny-Ålesund, Svalbard (78.92°N, 11.93°E), collected from March–May 2017–2023. BrO enhancements are positively correlated with aerosol extinction, indicating a close association with airborne particles, as supported by a Chemistry Transport Model (p-TOMCAT) simulations showing that heterogeneous recycling on aerosols is essential for sustaining elevated BrO levels. Five-day backward trajectories (0–3 km) showed significant BrO correlation with sea ice contact time, particularly over multi-year ice (MYI), which contributes comparably to first-year ice (FYI) in the total blowing-snow-sourced bromine flux, highlighting MYI's comparable importance to FYI in driving bromine explosion events. In addition, strong winds cause enhanced reactive bromine release from the sea ice. BrO and aerosol variability show a

seasonal shift, with sea ice dominating in early spring and open ocean influence increasing toward late spring. BrO correlated negatively with surface ozone and mercury, indicating that enhanced bromine drives both ozone and mercury depletion. In particular, observed BrO correlated positively with modelled blowing-snow-sourced sea salt aerosol and the corresponding bromine emission fluxes from blowing snow. Snowpack-sourced bromine fluxes also correlated with BrO, although disentangling release processes remains challenging."

The corresponding summary section of the manuscript has been modified as below:

"In this study, we integrated seven years (2017–2023) of MAX-DOAS BrO observations in Ny-Ålesund with GOME-2B measurements, meteorological data, p-TOMCAT simulations, and HYSPLIT backward trajectories to explore the sources and causes of variability in tropospheric BrO during polar spring (March to May). The MAX-DOAS BrO partial columns (0–4 km) show strong agreement with overpassing GOME-2B tropospheric columns within 45 km. The mean monthly BrO partial column exhibits a decreasing trend from March to May (1.97×10^{11} molecules cm^{-2} d^{-1}) with pronounced interannual variability. The most substantial short-term perturbations occur in early spring (March). Episodes of enhanced BrO frequently coincide with ODEs, highlighting the role of reactive bromine in Arctic atmospheric chemistry. In addition, BrO partial columns exhibit a significant negative correlation with GEM, with higher BrO generally associated with lower GEM concentrations, suggesting that enhanced bromine chemistry is closely involved in springtime atmospheric mercury depletion and influences regional oxidizing capacity.

Strong correlations between MAX-DOAS–retrieved BrO and aerosol extinction were observed at Ny-Ålesund, indicating a potential link between airborne particles and enhanced reactive bromine. Sensitivity simulations using p-TOMCAT further demonstrate that heterogeneous recycling of inactive bromine species (like HBr, HOBr and $BrONO_2$) on aerosols plays a dominant role in sustaining elevated BrO levels. For example, when heterogeneous reactivation was disabled, BrO partial columns dropped to approximately 15% of those when heterogeneous reactivation was on, strongly indicating that, without heterogeneous reactivation, pure gaseous-phase photochemical reactions alone are insufficient to maintain BEEs.

Backward trajectory analyses further revealed that enhanced BrO during BEEs is positively correlated with total sea ice contact time. Notably, the correlation coefficients between BrO and sea ice contact time are substantially larger (0.26–0.42) under high wind speed conditions (> 7 m s^{-1}) than under low wind speed conditions (0.10–0.19, ≤ 7 m s^{-1}). These results suggest that strong winds cause enhanced reactive bromine release from the sea ice surface, likely through the production of SSA from blowing snow, as previously proposed. This interpretation is further supported by the significant correlations between p-TOMCAT modelled SSA and retrieved BrO, as shown in Figure 13.

BrO and aerosol variability show a seasonal shift, with sea ice dominating in early spring and open ocean influence increasing toward late spring. However, over the entire period from March to May, BrO exhibits generally weak or negative correlations with air mass contact time with the open ocean and with the calculated bromine emission flux from sea spray. Weak or no correlations were also found with land contact time. These results indicate that neither the open ocean nor land serves as a major source of reactive bromine in Ny-Ålesund during the entire March–May period. This can be explained by the fact that, during BEEs, total sea ice contact

accounts for more than 50% of air mass contact time, whereas open ocean contact accounts for less than 10%.

Moreover, during BEEs, more than half of the air masses within the boundary layer originate from regions covered by MYI, particularly areas north of Greenland and the Canadian Arctic Archipelago. This is likely due to Svalbard's geographic location, which places it downwind of southward-flowing air masses approaching Ny-Ålesund, thereby allowing them to encounter MYI north of Greenland. Further analyses show that air masses during BEEs spend approximately 2.4 times longer in contact with MYI than with FYI, increasing to about 2.8 times under high wind speed (> 7 m s^{-1}) conditions. Accumulated blowing-snow-sourced bromine emissions over MYI contribute, on average, about 54% of the total sea-ice-sourced bromine. These results indicate that MYI plays an important and previously underappreciated role, comparable to that of first-year ice, in determining BEEs at Ny-Ålesund. Due to limitations in the model's representation of sea ice types and the lack of field data to constrain key parameters, such as snow salinity over MYI and FYI and the bromide depletion factor in SSA, we could not quantify their relative contributions to Ny-Ålesund BEEs or to BEEs across the whole Arctic. However, our findings still provide informative insights into the mechanisms and controlling factors of polar BEEs, which may be relevant for other coastal sites or across the pan-Arctic.

Note that this work could not rule out direct emissions of reactive bromine from the ice surface or the snowpack above it, given positive correlations between observed BrO and ice contact time, and between BrO and the parameterized reactive bromine flux from the snowpack. Notably, under high wind speed conditions, the correlation coefficients increase markedly compared with calm conditions, underscoring the dynamical influence on reactive bromine release, though the underlying microphysical processes remain unclear. Currently, the debate centres on two compelling mechanisms: the so-called "air-pumping" effect (Toyota et al., 2011) and the blowing-snow effect (Yang et al., 2008). Our findings highlight the need for quantitative measurements of snowpack emissions over sea ice, as well as boundary layer bromine budget analyses (Yang et al., 2024), to improve our understanding of the relevant processes, accurately constrain models in reproducing polar springtime BEEs and ODEs, and assess their climate impacts through effects on atmospheric oxidizing capacity."

Toyota, K., McConnell, J. C., Lupu, A., Neary, L., McLinden, C. A., Richter, A., Kwok, R., Semeniuk, K., Kaminski, J. W., Gong, S.-L., Jarosz, J., Chipperfield, M. P., and Sioris, C. E.: Analysis of reactive bromine production and ozone depletion in the Arctic boundary layer using 3-D simulations with GEM-AQ: inference from synoptic-scale patterns, Atmos. Chem. Phys., 11, 3949–3979, https://doi.org/10.5194/acp-11-3949-2011, 2011.

Yang, X., Pyle, J. A., and Cox, R. A.: Sea salt aerosol production and bromine release: Role of snow on sea ice, Geophys. Res. Lett., 35, L16815, https://doi.org/10.1029/2008gl034536, 2008.

Yang, X., Strong, K., Criscitiello, A. S., Santos-Garcia, M., Bognar, K., Zhao, X., Fogal, P., Walker, K. A., Morris, S. M., and Effertz, P.: Surface snow bromide and nitrate at Eureka, Canada, in early spring and implications for polar boundary layer chemistry, Atmos. Chem. Phys., 24, 5863–5886, https://doi.org/10.5194/acp-24-5863-2024, 2024.

Important points which should be addressed are:
Q1.2: what can be concluded from the study about the importance of initial release of reactive bromine compounds versus recycling? What is the role of aerosols in either of both processes?

A1.2: We performed a sensitivity simulation using p-TOMCAT in which heterogeneous reactivation on aerosols was disabled, while the initial release of reactive bromine was retained during March–May 2020. During the March–May 2020 BEEs, the mean BrO partial column (0–4 km) without heterogeneous reactivation was 1.788×10^{13} molecules cm^{-2}, corresponding to about 15% of that in the simulation with heterogeneous reactivation. The mean surface BrO VMR was 14.45 pptv in the simulation with heterogeneous reactivation, compared to 3.99 pptv without heterogeneous reactivation, corresponding to an enhancement factor of 3.62. This indicates that the initial release alone is insufficient to sustain elevated BrO levels, and that heterogeneous recycling on aerosols plays a critical role in maintaining high BrO levels. When heterogeneous reactivation was included, the total inorganic bromine (Br_y, including BrO, Br, Br_2, $BrNO_2$, $BrONO_2$, HBr, and HOBr) only increased by ~20% (Fig. 1a), which is attributed to the alternation of bromine-containing species partitions. However, the BrO/Br_y ratio significantly increased by a factor of ~6.7, from 0.06 to 0.40 (Fig. 1b), demonstrating the importance of heterogeneous reactivation in enhancing BrO partitioning within Br_y.

The enhanced BrO associated with heterogeneous reactivation mainly arises from two factors: (i) efficient conversion of bromine reservoir species (e.g. HBr, HOBr, and $BrONO_2$) into reactive bromine, leading to increased BrO partitioning, and (ii) reduced depositional loss of Br-containing species. Overall, our results indicate that while the initial release of reactive bromine serves as a reservoir, heterogeneous recycling on aerosols plays a dominant role in sustaining high BrO levels.

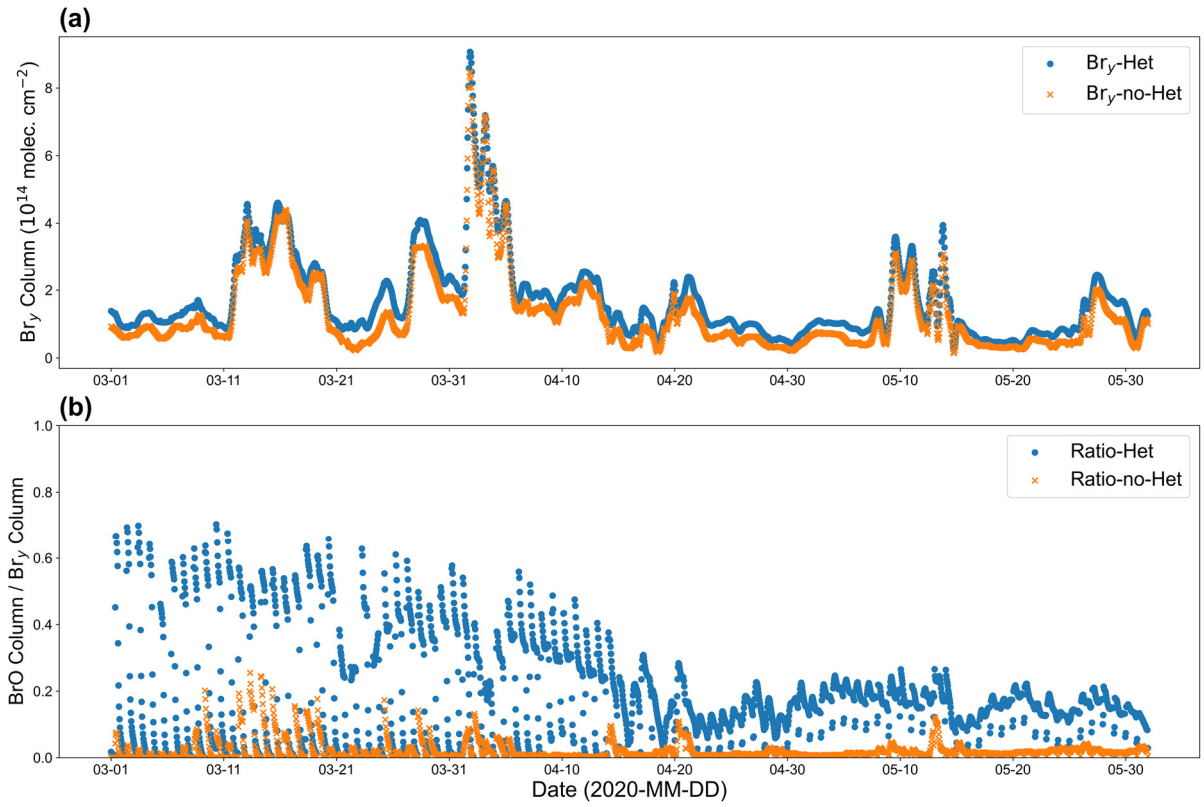

Figure 1. Time series during the March–May 2020 BEEs. (a) Simulated Br_y partial column (0–4 km) with heterogeneous reactivation (blue) and without heterogeneous reactivation (orange). (b) Simulated BrO (0–4 km) to Br_y (0–4 km) partial column ratio for the two experiments.

The corresponding section of the manuscript has been modified as below (P25, lines 532–545):

"In addition, we performed a sensitivity experiment for the period of March–May 2020 using p-TOMCAT, in which heterogeneous reactivation on aerosols was disabled, while the initial release of reactive bromine from blowing snow was retained. During the March–May 2020 BEEs, the mean BrO partial column (0–4 km) without heterogeneous reactivation was 1.788 × 10^{13} molecules cm^{-2}, only about 15% of the value with heterogeneous reactivation. The mean surface BrO VMR was 14.45 pptv in the simulation with heterogeneous reactivation, compared to 3.99 pptv without heterogeneous reactivation, corresponding to an enhancement factor of 3.62. This indicates that the initial release alone is insufficient to sustain elevated BrO levels without help from heterogeneous recycling on aerosols. When heterogeneous reactivation was included, the total inorganic bromine Br_y (including BrO, Br, Br_2, $BrNO_2$, $BrONO_2$, HBr, and HOBr) increased by ~20% (Fig. S18a), and the BrO/Br_y ratio increased by a factor of ~6.7, from 0.06 to 0.40 (Fig. S18b). This demonstrates that heterogeneous reactivation substantially enhances both the total inorganic bromine level and the partitioning of BrO within Br_y. Heterogeneous reactivation affects bromine chemistry in two ways: (i) efficient conversion of bromine reservoir species into reactive bromine, leading to increased BrO partitioning, and (ii) consequently reduced depositional loss of Br-containing species from the air. Overall, while the initial release of reactive bromine serves as a reservoir of bromine, heterogeneous recycling on aerosols plays a dominant role in sustaining high BrO levels."

Q1.3: In Spitsbergen, relatively infrequent BEE occur. How representative are the results in general and for other locations?

A1.3: Spitsbergen is located in a geographically special environment. During polar spring, the region north of Ny-Ålesund is typically covered by sea ice, whereas the area to the south is generally open ocean. In addition, Ny-Ålesund is located in a valley, which typically channels the local winds into northwesterly or southeasterly directions. BEEs in Ny-Ålesund are relatively infrequent, which is consistent with the low number of surface ozone depletion hours observed at the nearby Zeppelin station, as shown in Figure 2.

Given this unique geographical and meteorological setting, the occurrence and characteristics of BEE events in Ny-Ålesund may differ from those at other Arctic locations. However, our findings can still provide useful qualitative insights into the mechanisms and controlling factors of BEE events, which may be relevant for other Arctic coastal sites with similar environmental conditions.

The modifications described above have been implemented in the manuscript (P37, lines 753–755).

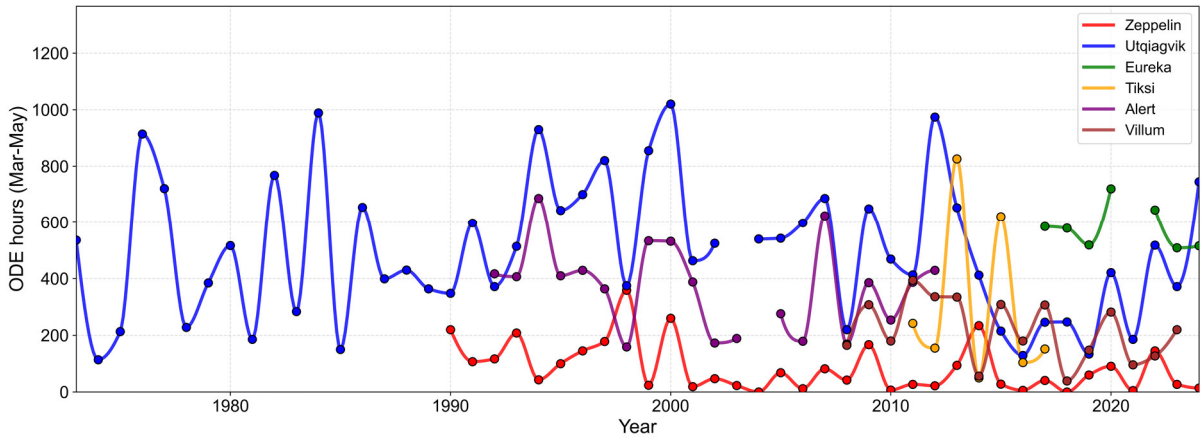

Figure 2. Time series of the annual number of hours with surface ozone depletion events (< 10 ppbv) during March–May from 1973 to 2024 at six Arctic stations: Zeppelin, Utqiagvik, Eureka, Tiksi, Alert, and Villum. Ozone data were obtained from the EBAS database (https://ebas-data.nilu.no/).

Q1.4: what is the impact of enhanced BrO on GEM? (the GEM data are used in the study, but no further conclusions are drawn). This should be explored and also discussed in the abstract and conclusions.

A1.4: Thank you for the comment. We have added further analyses of GEM data in the revised manuscript (Fig. 3–4). Previous studies have suggested that a large proportion of springtime atmospheric mercury depletion events observed at Ny-Ålesund is likely associated with the long-range transport of air masses containing depleted Hg(0) from regions over the Arctic Ocean (Gauchard et al., 2005; Sommar et al., 2007; Berg et al., 2013). During 2017–2023, the mean GEM concentration in spring was 1.35 ng m^{-3} (Fig. 3i–j), which is comparable to the

mean value of 1.38 ng m^{-3} observed at Ny-Ålesund during 2011–2015 (Angot et al., 2016). At the monthly scale, GEM variations also do not show a clear relationship with BrO partial columns. The impact of bromine on GEM is shown in Fig. 4c–d. When GEM concentrations are low, the corresponding mean and median BrO partial columns are generally higher than those observed when GEM are high. Figure 4c presents boxplots of BrO partial columns categorized by different GEM concentration ranges (< 0.4, 0.4–0.8, 0.8–1.2, and > 1.2 ng m^{-3}). The highest mean and median BrO partial columns occur in the lowest GEM range (< 0.4 ng m^{-3}) and decrease progressively with increasing GEM concentrations. In addition, BrO partial columns exhibit significant negative correlations with GEM ($r = -0.28$, $p < 0.0001$; Fig. 4d). These results indicate that enhanced BrO partial columns are closely associated with the depletion of GEM, underscoring the key role of bromine chemistry in Arctic springtime atmospheric processes.

The modifications described above have been implemented in the manuscript (P13, lines 354–365).

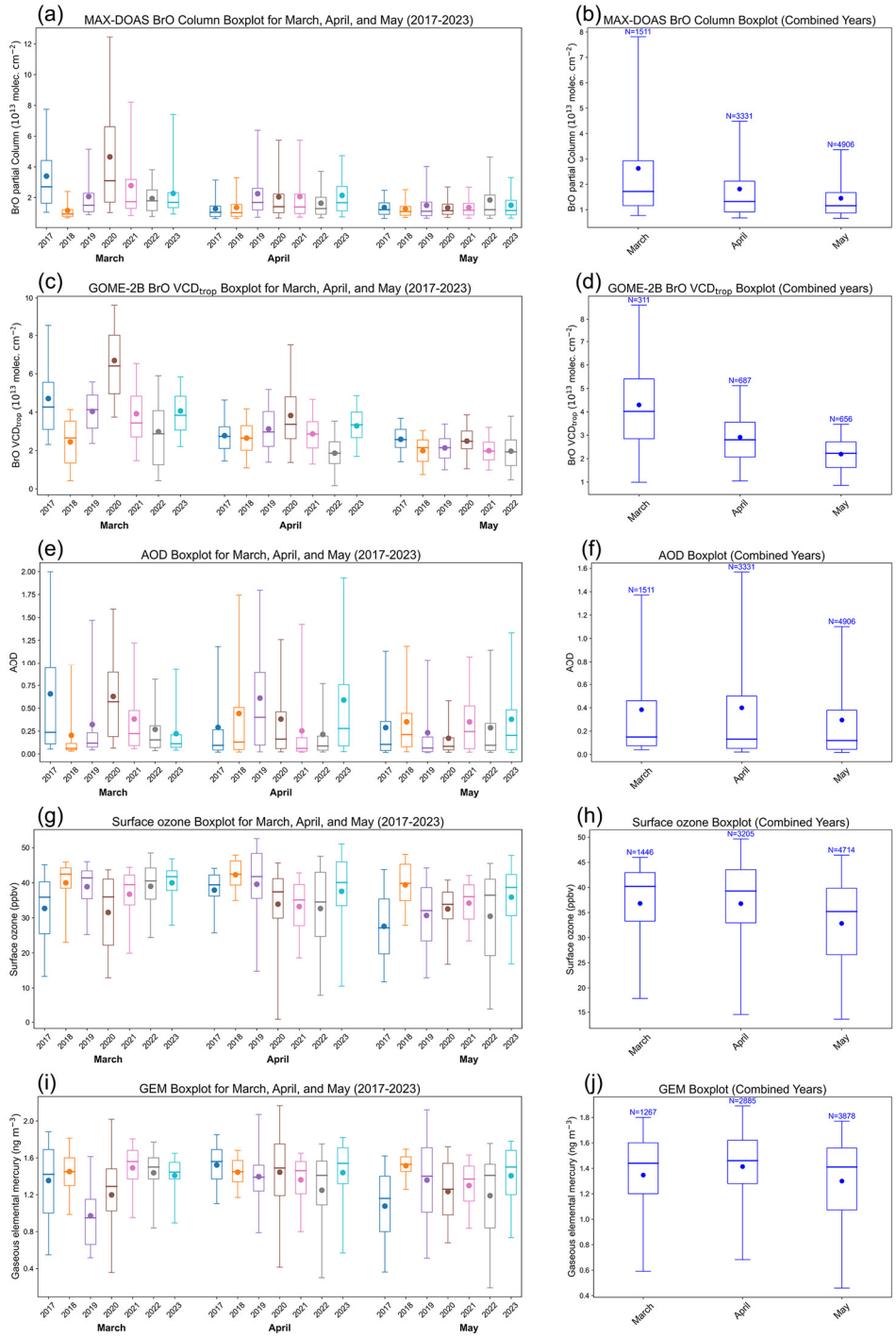

Figure 3. Left panel: boxplots of monthly MAX-DOAS-retrieved BrO partial columns (a), GOME-2B tropospheric BrO columns (c), MAX-DOAS-retrieved AOD (e), surface ozone (g), and GEM (i) for March–May in each year from 2017 to 2023 in Ny-Ålesund; right panel: multiyear monthly MAX-DOAS BrO (b), GOME-2B BrO (d), MAX-DOAS AOD (f), ozone (h), and GEM (j). The boxes represent the 25th–75th percentile range, the whiskers indicate the 5th–95th percentile range, the dots represent the mean values, and the horizontal lines in the boxes indicate the median values. N is the number of hours counted. To ensure consistency with the MAX-DOAS BrO observations, only hours with valid surface ozone and GEM data during BrO observation periods were considered. Note that MAX-DOAS and GOME-2B BrO are not sampled at exactly the same times.

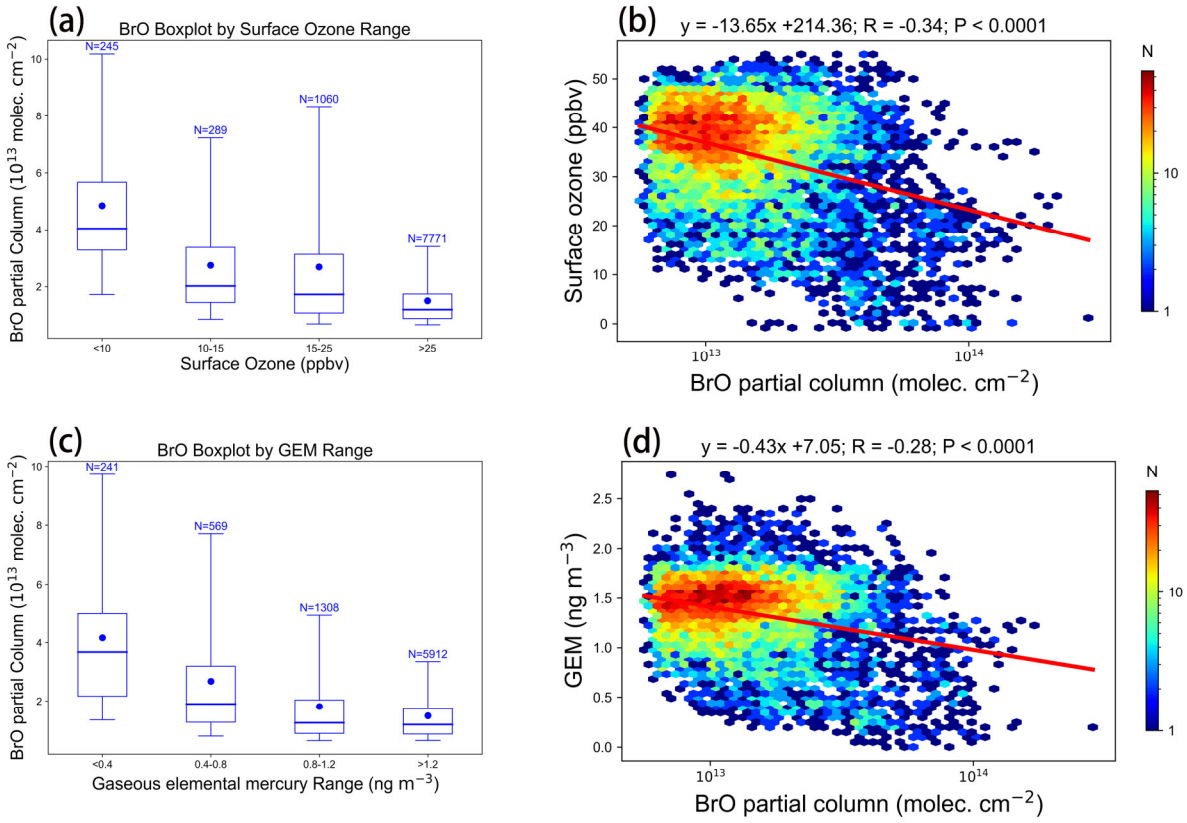

Figure 4. Relationship between BrO partial columns and surface ozone and gaseous elemental mercury (GEM) from March to May during 2017–2023. (a) Boxplots of BrO partial columns corresponding to different surface ozone concentration ranges. (b) Correlation analysis between BrO partial column and surface ozone. (c) Boxplots of BrO partial columns corresponding to different GEM concentration ranges. (d) Correlation analysis between BrO partial column and GEM. The boxes represent the 25th–75th percentile range, the whiskers indicate the 5th–95th percentile range, the dots represent the mean values, and the horizontal lines in the boxes indicate the median values. N is the number of hours counted.

Angot, H., Dastoor, A., De Simone, F., Gårdfeldt, K., Gencarelli, C. N., Hedgecock, I. M., Langer, S., Magand, O., Mastromonaco, M. N., Nordstrøm, C., Pfaffhuber, K. A., Pirrone, N., Ryjkov, A., Selin, N. E., Skov, H., Song, S., Sprovieri, F., Steffen, A., Toyota, K., Travnikov, O., Yang, X., and Dommergue, A.: Chemical cycling and deposition of atmospheric mercury in polar regions: review of recent measurements and comparison with models, Atmos. Chem. Phys., 16, 10735–10763, https://doi.org/10.5194/acp-16-10735-2016, 2016.

Berg, T., Pfaffhuber, K. A., Cole, A. S., Engelsen, O., and Steffen, A.: Ten-year trends in atmospheric mercury concentrations, meteorological effects and climate variables at Zeppelin, Ny-Ålesund, Atmos. Chem. Phys., 13, 6575–6586, doi:10.5194/acp-13-6575-2013, 2013.

Gauchard, P.-A., Aspmo, K., Temme, C., Steffen, A., Ferrari, C., Berg, T., Ström, J., Kaleschke, L., Dommergue, A., Bahlmann, E., Magand, O., Planchon, F., Ebinghaus, R., Banic, C., Nagorski, S., Baussand, P., and Boutron, C.: Study of the origin of atmospheric mercury depletion events recorded in Ny-Ålesund, Svalbard, spring 2003, Atmos. Environ., 39, 7620–7632, doi:10.1016/j.atmosenv.2005.08.010, 2005.

Sommar, J., Wängberg, I., Berg, T., Gårdfeldt, K., Munthe, J., Richter, A., Urba, A., Wittrock, F., and Schroeder, W. H.: Circumpolar transport and air-surface exchange of atmospheric mercury at Ny-Ålesund (79◦ N), Svalbard, spring 2002, Atmos. Chem. Phys., 7, 151–166, doi:10.5194/acp-7-151-2007, 2007.

Minor comments:

Q1.5: clouds can have a strong influence on both satellite and ground-based observations. How are clouds treated in both analyses? Are the data filtered for cloud effects? Are cloud effects corrected?

A1.5: Cloud effects are indeed an important issue for both ground-based and satellite observations in polar regions. For the MAX-DOAS measurements, no cloud filter was applied to the retrieved profiles because clouds and aerosol (including blowing snow SSA) cannot be clearly distinguished. Applying a cloud filter would therefore prevent a reliable investigation of the impact of blowing snow SSA on BrO. As a result, part of the reported aerosol optical depth (AOD) in this study may be attributed to extinction by clouds rather than by aerosols or snow particles (Frieß et al., 2023).

For the GOME-2B satellite data, clouds are neither filtered nor corrected in the BrO product. Over dark surfaces, the absence of cloud filtering can lead to a substantial underestimation of near-surface BrO. Over bright surfaces, photons can penetrate cloud layers, undergo absorption below the clouds, and return through the cloud with a certain probability. Although clouds affect the air mass factors of satellite retrievals, the magnitude of this impact depends on surface albedo, viewing geometry, and the vertical distribution of BrO and clouds, and is generally smaller than might be expected. As demonstrated in previous studies (e.g., Blechschmidt et al., 2016), the impact of clouds on BrO retrievals is much smaller over bright surfaces.

The modifications described above have been implemented in the manuscript (P8, lines 217–221; P9, lines 248–253).

Blechschmidt, A.-M., Richter, A., Burrows, J. P., Kaleschke, L., Strong, K., Theys, N., Weber, M., Zhao, X., and Zien, A.: An exemplary case of a bromine explosion event linked to cyclone development in the Arctic, Atmos. Chem. Phys., 16, 1773–1788, https://doi.org/10.5194/acp-16-1773-2016, 2016.

Frieß, U., Kreher, K., Querel, R., Schmithüsen, H., Smale, D., Weller, R., and Platt, U.: Source mechanisms and transport patterns of tropospheric bromine monoxide: findings from long-term multi-axis differential optical absorption spectroscopy measurements at two Antarctic stations, Atmospheric Chemistry and Physics, 23, 3207–3232, https://doi.org/10.5194/acp-23-3207-2023, 2023.

Q1.6: Fig. 3: how does MAX-DOAS AOD compare to AOD from AERONET? AERONET data at Ny-Ålesund are available for several years. Such a comparison is needed to strengthen the confidence in the MAX-DOAS results. Also, a correlation analysis between AERONET

AOD and BrO should be performed (like in Fig. 7).

A1.6: We thank the reviewer for this valuable suggestion. We have performed a comparison between MAX-DOAS AOD and AERONET AOD at Ny-Ålesund (https://aeronet.gsfc.nasa.gov/) (Figure 5). MAX-DOAS AOD was retrieved at 361 nm, while the AERONET AODs at 380 and 340 nm were converted to 361 nm based on the Ångström exponent. The two resulting AERONET AODs at 361 nm were then averaged, and this averaged AERONET AOD was used for the comparison with MAX-DOAS AOD. The overall correlation coefficient is R = 0.14 ($p < 0.001$). To further investigate the influence of sky conditions, we selected two clear-sky days (Figures 6a–b) and two cloudy days (Figures 6c–d) using sky camera observations (https://doi.org/10.21334/NPOLAR.2013.9FD6DAE0). Under clear-sky conditions (Figures 6e–f), MAX-DOAS AOD shows a significant positive correlation with AERONET AOD, with R ranging from 0.72 to 0.83. In these cases, AERONET AOD is generally higher than MAX-DOAS AOD, because AERONET measures the total AOD (including both tropospheric and stratospheric contributions), whereas MAX-DOAS mainly retrieves aerosol extinction in the lower troposphere (0–4 km).

In contrast, under low-visibility conditions or when clouds are present several kilometers away from the instrument (Figures 6g and 6j), no significant positive correlation is found, and MAX-DOAS AOD is often higher than AERONET AOD (Figures 6c–d). This discrepancy is mainly attributed to the different observation geometries. AERONET relies on direct-sun measurements, whereas MAX-DOAS is based on scattered sunlight and measures air masses extending horizontally over several kilometers. Consequently, the two instruments generally sample different atmospheric air masses. These results indicate that AERONET AOD may be suitable for evaluating MAX-DOAS AOD only under clear-sky conditions, when aerosol extinction in the boundary layer dominates the tropospheric AOD (Frieß et al., 2016; Davis et al., 2020).

In addition, we have performed correlation analyses between MAX-DOAS BrO partial columns and MAX-DOAS AOD (Figure 7a) and AERONET AOD (Figure 7b) during March–May for the period 2017–2023. MAX-DOAS BrO partial columns show significant positive correlations with MAX-DOAS AOD (R = 0.54) and AERONET AOD (R = 0.32). These results further support a close association between BrO enhancements and airborne particles.

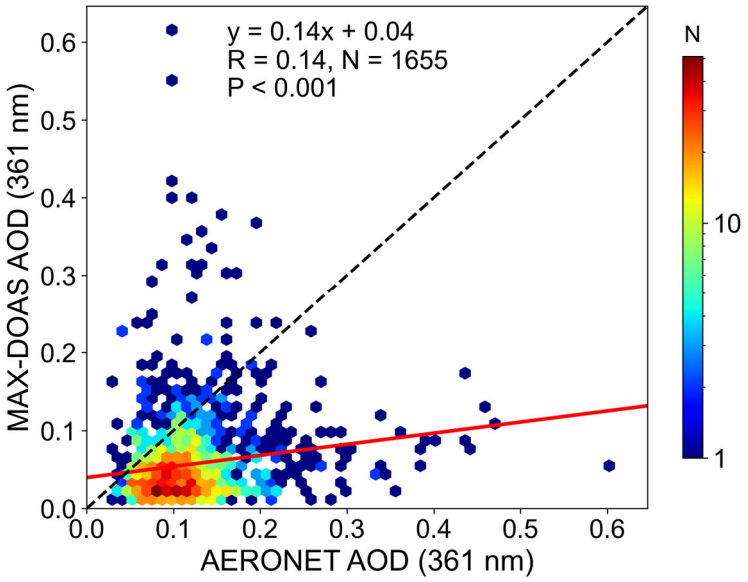

Figure 5. Correlation analysis between MAX-DOAS AOD and AERONET AOD during March–May for the 2017–2023 period.

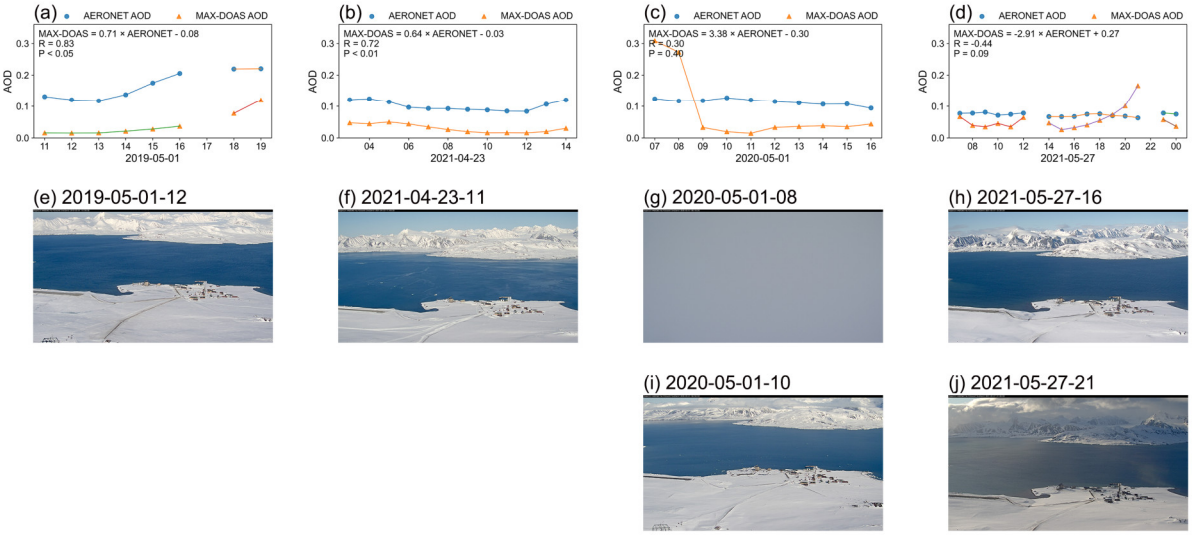

Figure 6. Time series of MAX-DOAS and AERONET AOD under clear-sky (a, b) and cloudy (c, d) conditions at Ny-Ålesund. Panels (e)–(j) show camera images taken at Ny-Ålesund on the corresponding days. All times are given in UTC.

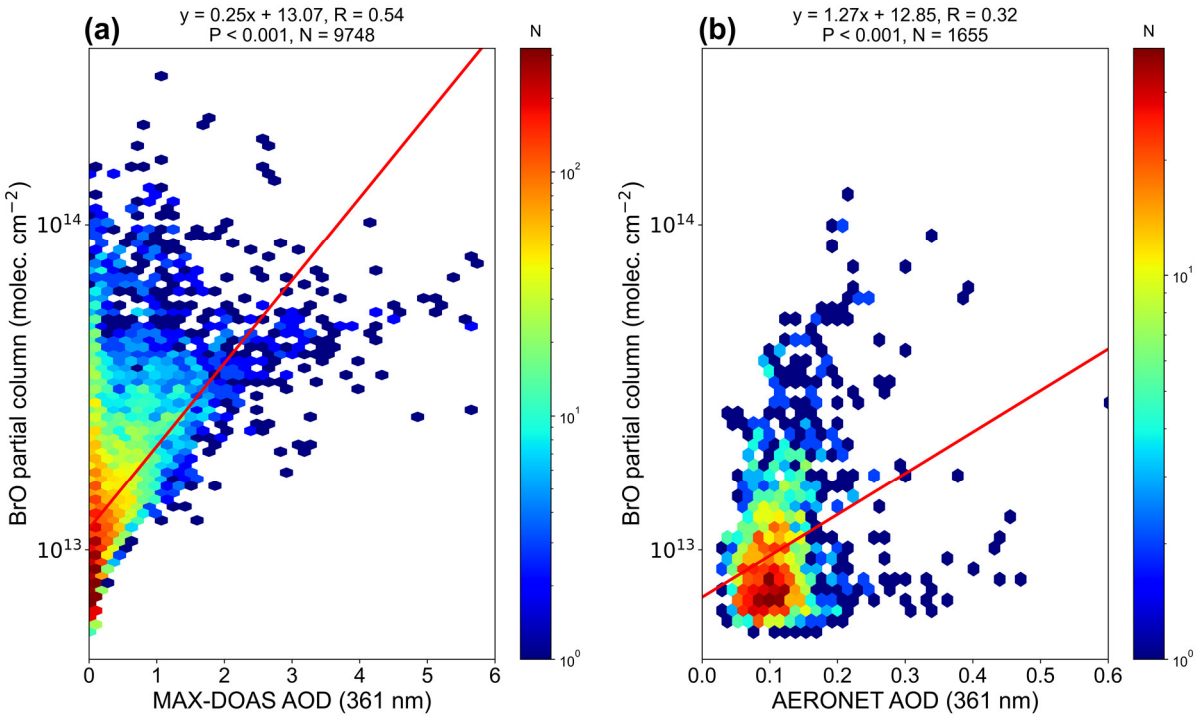

Figure 7. Correlation analysis between MAX-DOAS BrO partial columns and MAX-DOAS AOD (a) and AERONET AOD (b) during March–May for the 2017–2023 period.

The corresponding section of the manuscript has been modified as below (P19, lines 480–493):

"In addition, we compared MAX-DOAS AOD with collocated AERONET observations at Ny-Ålesund (https://aeronet.gsfc.nasa.gov/). MAX-DOAS AOD was retrieved at 361 nm, while AERONET AODs at 340 and 380 nm were converted to 361 nm using the Ångström exponent and then averaged. During March–May (2017–2023), only a weak correlation was found ($R = 0.14$, $p < 0.001$) (Fig. S15). However, under clear-sky conditions, MAX-DOAS AOD shows a strong positive correlation with AERONET AOD ($R = 0.72–0.83$) (Fig. S16a–b), whereas under cloudy or low-visibility conditions the correlation becomes insignificant (Fig. S16c–d). The discrepancy is mainly attributed to AERONET measures the total AOD (including both tropospheric and stratospheric contributions), whereas MAX-DOAS mainly retrieves aerosol extinction in the lower troposphere (0–4 km). AERONET relies on direct-sun measurements, whereas MAX-DOAS is based on scattered sunlight and measures air masses extending horizontally over several kilometers. Consequently, the two instruments generally sample different atmospheric air masses. These results indicate that AERONET AOD may be suitable for evaluating MAX-DOAS AOD only under clear-sky conditions, when aerosol extinction in the boundary layer dominates the tropospheric AOD (Frieß et al., 2016; Davis et al., 2020). Furthermore, significant positive correlations were found between MAX-DOAS BrO partial columns and MAX-DOAS AOD ($R = 0.54$) as well as AERONET AOD ($R = 0.32$) during March–May (2017–2023) (Fig. S17), indicating a close association between BrO enhancements and airborne particles."

Davis, Z. Y. W., Frieß, U., Strawbridge, K. B., Aggarwaal, M., Baray, S., Schnitzler, E. G., Lobo, A., Fioletov, V. E., Abboud, I., McLinden, C. A., Whiteway, J., Willis, M. D., Lee, A.

K. Y., Brook, J., Olfert, J., O'Brien, J., Staebler, R., Osthoff, H. D., Mihele, C., and McLaren, R.: Validation of MAX-DOAS retrievals of aerosol extinction, SO2, and NO2 through comparison with lidar, sun photometer, active DOAS, and aircraft measurements in the Athabasca oil sands region, Atmos. Meas. Tech., 13, 1129–1155, https://doi.org/10.5194/amt-13-1129-2020, 2020.

Frieß, U., Klein Baltink, H., Beirle, S., Clémer, K., Hendrick, F., Henzing, B., Irie, H., de Leeuw, G., Li, A., Moerman, M. M., van Roozendael, M., Shaiganfar, R., Wagner, T., Wang, Y., Xie, P., Yilmaz, S., and Zieger, P.: Intercomparison of aerosol extinction profiles retrieved from MAX-DOAS measurements, Atmos. Meas. Tech., 9, 3205–3222, https://doi.org/10.5194/amt-9-3205-2016, 2016.

Q1.7: Fig. 3: also the BrO results from GOME and the in situ results for GEM should be included.

A1.7: We have included the GOME-2B BrO tropospheric column data and the GEM measurements in Figure 3. The declining trend in GOME-2B BrO from March to May is also reflected in all central-tendency metrics (mean, median, 75th, and 95th percentiles) (Figure 3d). For example, the seven-year average decreasing rate is 4.63×10^{11} molecules cm^{-2} d^{-1} from March to April and 2.40×10^{11} molecules cm^{-2} d^{-1} from April to May, yielding an overall rate of 3.52×10^{11} molecules cm^{-2} d^{-1} from March to May. The discussion of GEM results is provided in our response to Q1.4.

The corresponding section of the manuscript has been modified as below (P12, lines 327–330):

"The declining trend in GOME-2B BrO from March to May is also reflected in all central-tendency metrics (mean, median, 75th, and 95th percentiles) (Figure 3d). For example, the seven-year average decreasing rate is 4.63×10^{11} molecules cm^{-2} d^{-1} from March to April and 2.40×10^{11} molecules cm^{-2} d^{-1} from April to May, yielding an overall rate of 3.52×10^{11} molecules cm^{-2} d^{-1} from March to May."

Q1.8: In Fig. 4 the BrO values for different O3 mixing ratio bins are shown. But it would also be important to see the relationship between individual observations or daily averages. How do these correlations look like for the whole time series (2017-2023)?

A1.8: We have added Figure 4b, which presents the correlation analysis between MAX-DOAS BrO partial columns and surface ozone during March–May for the 2017–2023 period. The correlation coefficient for the whole time series is $R = -0.34$ ($p < 0.0001$), further supporting that enhanced BrO partial columns are closely associated with the depletion of surface ozone.

The corresponding section of the manuscript has been modified as below (P12, lines 350–352):

"The correlation coefficient between MAX-DOAS BrO partial columns and surface ozone for the whole time series is $R = -0.34$ ($p < 0.0001$) (Figure 4b), further supporting that enhanced BrO partial columns are closely associated with the depletion of surface ozone."

Q1.9: Section 3.3: in 2020 the BrO values were rather high. I suggest to add another year with relatively low values to better cover the different conditions. 2019 might be well suited because of the rather high number of measurements.

A1.9: We thank the reviewer for this valuable suggestion. We have added an additional year (2019), which is characterized by relatively lower BrO values, to better represent different atmospheric conditions. Specifically, we have added Figures 8 and 9 showing the time series and correlation analyses for March–May 2019, and extended the discussion in Section 3.3 accordingly.

In 2019, BrO partial columns still exhibited negative correlations with surface ozone ($r = -0.26$) and GEM ($r = -0.18$), as well as with air temperature ($r = -0.25$) and pressure ($r = -0.27$). A positive correlation with wind speed was also observed ($r = 0.18$), indicating the influence of blowing-snow-sourced SSA on reactive bromine release.

Similar to 2020, BrO VMR in 2019 showed a strong positive correlation with aerosol extinction ($r = 0.52$), further supporting a close link between atmospheric particles and elevated BrO levels. In addition, BrO exhibited a significant positive correlation with relative humidity in 2019 ($r = 0.36$). This positive relationship may be associated with enhanced heterogeneous uptake of HOBr on acidified sea-salt aerosols under humid conditions, as the reactive uptake coefficient increases with relative humidity and reaches a maximum at a relative humidity of approximately 75–80% (Pratte and Rossi, 2006; Roberts et al., 2014). Moreover, hygroscopic growth of sea-salt aerosols at high humidity may further influence heterogeneous reaction efficiencies (Zieger et al., 2017; Tang et al., 2019).

Back-trajectory analysis for 2019 also revealed positive correlations between BrO and total sea ice contact time ($r = 0.18$), as well as with MYI ($r = 0.12$) and FYI ($r = 0.14$,), whereas no significant correlation was found with open ocean contact ($r = 0.04$). Although these correlations were weaker than those observed in 2020, they consistently indicate that sea ice regions remained an important source of reactive bromine in both years.

Overall, the comparison between 2019 and 2020 demonstrates that, despite substantial interannual differences in BrO abundance, the dominant relationships among BrO, aerosols, sea ice contact, and meteorological conditions are consistent, indicating robust underlying physical-chemical processes that determine polar bromine chemistry across different years.

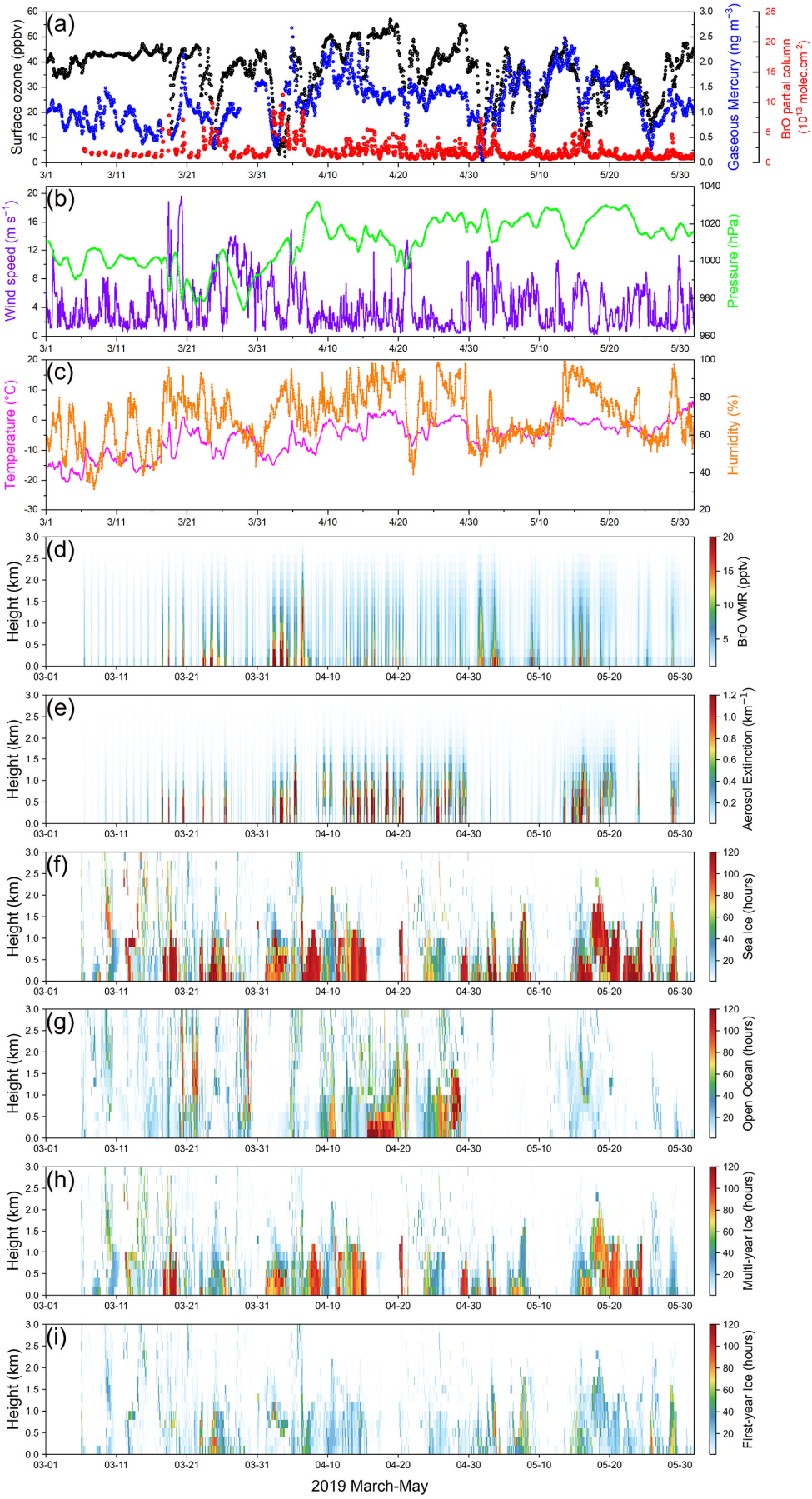
(a)
Surface ozone (ppbv)
Gaseous Mercury (ng m^{-3})
BrO partial column (10^{13} molec.cm^{-2})
(b)
Wind speed (m s^{-1})
Pressure (hPa)
(c)
Temperature (°C)
Humidity (%)
(d)
Height (km)
BrO VMR (pptv)
(e)
Aerosol Extinction (km^{-1})
(f)
Sea Ice (hours)
(g)
Open Ocean (hours)
(h)
Multi-year Ice (hours)
(i)
First-year Ice (hours)
3/1
3/11
3/21
3/31
4/10
4/20
4/30
5/10
5/20
5/30
03-01
03-11
03-21
03-31
04-10
04-20
04-30
05-10
05-20
05-30
2019 March-May

Figure 8. Panel (a) surface ozone (black dots), gaseous mercury (Hg(0)) (blue dots) and BrO partial column (red dots); (b) wind speed (purple line), pressure (green line); (c) temperature (pink line), relative humidity (orange line); (d) BrO profiles; (e) aerosol extinction profiles; (f) total sea ice contact time profiles; (g) open ocean contact time profiles; (h) MYI contact time profiles; and (i) FYI contact time profiles between March and May 2019 in Ny-Ålesund. All data are shown at hourly resolution.

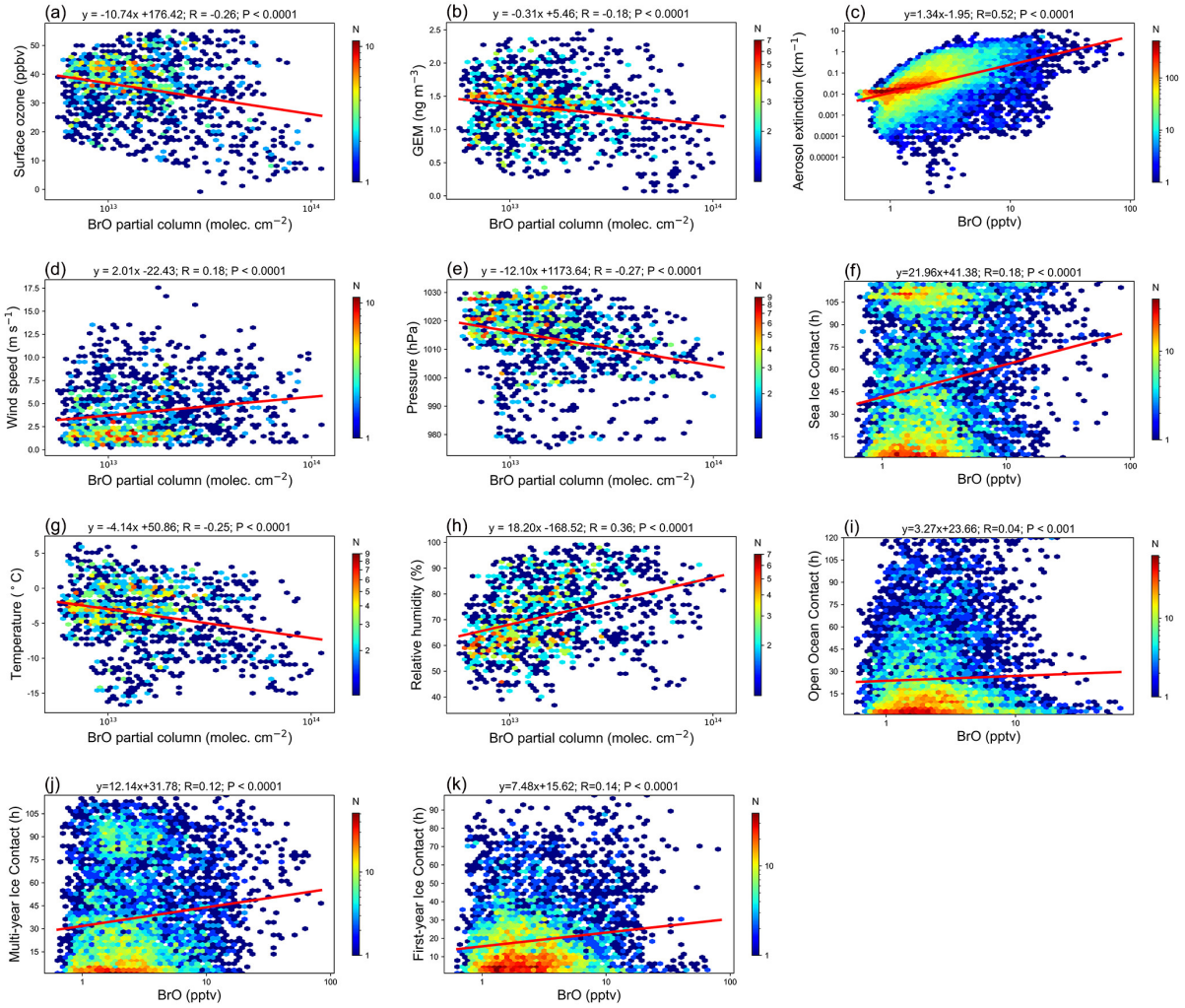

Figure 9. Correlation analysis between BrO and various parameters during March–May 2019. BrO partial column correlations are shown for surface ozone (a), GEM (b), wind speed (d), pressure (e), temperature (g), and relative humidity (h). BrO VMR profile correlations are shown for aerosol profiles (c), total sea ice contact time (f), open ocean contact time (i), MYI contact time (j), and FYI contact time (k).

The corresponding section of the manuscript has been modified as below (P18, lines 440–458):

"To examine whether the identified relationships are robust under different atmospheric conditions, we further analyzed data from 2019, which is characterized by relatively lower BrO levels. Figures 8 and 9 present the time series and correlation analyses for March–May 2019. In 2019, BrO partial columns still exhibited negative correlations with surface ozone ($r = -0.26$) and GEM ($r = -0.18$), as well as with air temperature ($r = -0.25$) and pressure ($r = -0.27$). A positive correlation with wind speed was also observed ($r = 0.18$), indicating a continued influence of blowing-snow-sourced SSA on reactive bromine release. Similar to 2020, BrO VMR in 2019 showed a strong positive correlation with aerosol extinction ($r = 0.52$), further

supporting a close link between atmospheric particles and elevated BrO levels. In addition, BrO exhibited a significant positive correlation with relative humidity in 2019 (r = 0.36). This positive relationship may be associated with enhanced heterogeneous uptake of HOBr on acidified sea-salt aerosols under humid conditions, as the reactive uptake coefficient increases with relative humidity and reaches a maximum at a relative humidity of approximately 75–80% (Pratte and Rossi, 2006; Roberts et al., 2014). Moreover, hygroscopic growth of sea-salt aerosols at high humidity may further influence heterogeneous reaction efficiencies (Zieger et al., 2017; Tang et al., 2019).

Back-trajectory analysis for 2019 also revealed positive correlations between BrO and total sea ice contact time (r = 0.18), as well as with MYI (r = 0.12) and FYI (r = 0.14,), whereas no significant correlation was found with open ocean contact (r = 0.04). Although these correlations were weaker than those observed in 2020, they consistently indicate that sea ice regions remained an important source of reactive bromine in both years. Overall, the comparison between 2019 and 2020 demonstrates that, despite substantial interannual differences in BrO abundance, the dominant relationships among BrO, aerosols, sea ice contact, and meteorological conditions are consistent, indicating robust underlying physical-chemical processes that determine polar bromine chemistry across different years."

Pratte, P. and Rossi, M. J.: The heterogeneous kinetics of HOBr and HOCl on acidified sea salt and model aerosol at 40–90% relative humidity and ambient temperature, Phys. Chem. Chem. Phys., 8, 3988–4001, 2006.

Roberts, T. J., Jourdain, L., Griffiths, P. T., and Pirre, M.: Re-evaluating the reactive uptake of HOBr in the troposphere with implications for the marine boundary layer and volcanic plumes, Atmos. Chem. Phys., 14, 11185–11199, https://doi.org/10.5194/acp-14-11185-2014, 2014.

Tang, M., Chan, C. K., Li, Y. J., Su, H., Ma, Q., Wu, Z., Zhang, G., Wang, Z., Ge, M., Hu, M., He, H., and Wang, X.: A review of experimental techniques for aerosol hygroscopicity studies, Atmos. Chem. Phys., 19, 12631–12686, https://doi.org/10.5194/acp-19-12631-2019, 2019.

Zieger, P., Vaisanen, O., Corbin, J. C., Partridge, D. G., Bastelberger, S., Mousavi-Fard, M., Rosati, B., Gysel, M., Krieger, U. K., Leck, C., Nenes, A., Riipinen, I., Virtanen, A., and Salter, M. E.: Revising the hygroscopicity of inorganic sea salt particles, Nat. Commun., 8, 15883, https://doi.org/10.1038/ncomms15883, 2017.

Q1.10: Fig. 7: the correlation between BrO (and aerosols) with the ocean and sea ice contact times should be performed separately for the first and second half of the shown period. It seems from Fig. 6 that there is a high correlation between the occurrence of ocean contact and BrO events for the second half of the time period. Is there an explanation for the different behaviors in both periods?

A1.10: We conducted separate correlation analyses for the first and second halves of the observation period, and the results are shown in Figs. 10–13. For both 2019 and 2020, BrO VMR exhibits a stronger positive correlation with sea ice contact time during the first half of the period (March 1–April 15) than during the second half (April 16–May 31). In 2020, the

correlation decreases from 0.52 in the first half to 0.21 in the second half, and in 2019 from 0.39 to 0.07. This suggests that sea ice contact is more closely associated with BrO variability in early spring. In contrast, during the second half of the period, BrO VMR and aerosol extinction tend to show enhanced positive correlations with open ocean contact time. For example, in 2020, the correlation between BrO VMR and open ocean contact increases from −0.31 in the first half to 0.27 in the second half, while that for aerosol extinction increases from −0.14 to 0.34. Similar tendencies are also observed in 2019. These differences is related to the seasonal evolution of sea ice conditions. In early spring, extensive and stable sea ice coverage, associated with photochemical processes in surface snow and with blowing snow, may lead to a stronger association between BrO and sea ice contact. Toward late spring, gradual sea ice melting and retreat increase the extent of open ocean, which may enhance the influence of open ocean regions on reactive bromine and aerosol variability. Overall, our time series analysis suggests a seasonal shift in the relative influence of sea ice and open ocean contact on BrO and aerosol variability from early to late spring.

The modifications described above have been implemented in the manuscript (P19, lines 459–472).

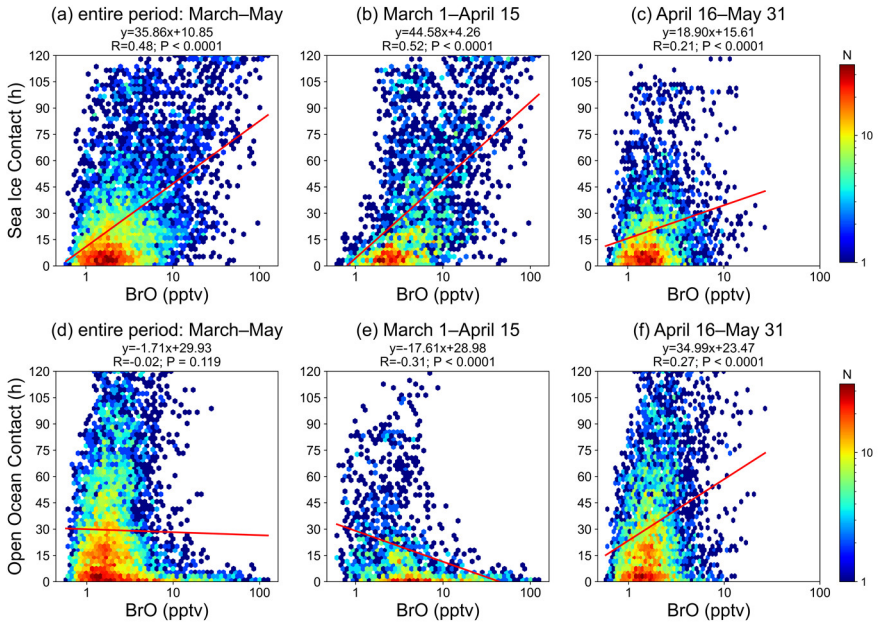

Figure 10. Correlation analysis between BrO VMR and surface contact times over sea ice and open ocean in 2020. Panels (a–c) show the correlation between BrO VMR and sea ice contact time: (a) for the entire period from March to May, (b) for the first half of the period (March 1–April 15), and (c) for the second half (April 16–May 31). Panels (d–f) show the correlation between BrO VMR and open ocean contact time: (d) for the entire period, (e) for the first half, and (f) for the second half.

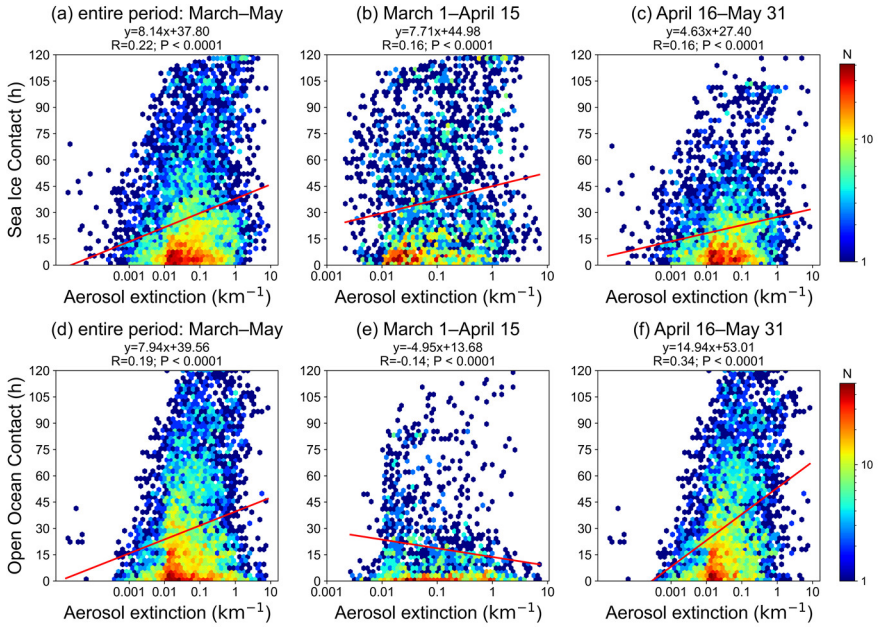

Figure 11. Correlation analysis between aerosol extinction and surface contact times over sea ice and open ocean in 2020. Panels (a–c) show the correlation between aerosol extinction and sea ice contact time: (a) for the entire period from March to May, (b) for the first half of the period (March 1–April 15), and (c) for the second half (April 16–May 31). Panels (d–f) show the correlation between aerosol extinction and open ocean contact time: (d) for the entire period, (e) for the first half, and (f) for the second half.

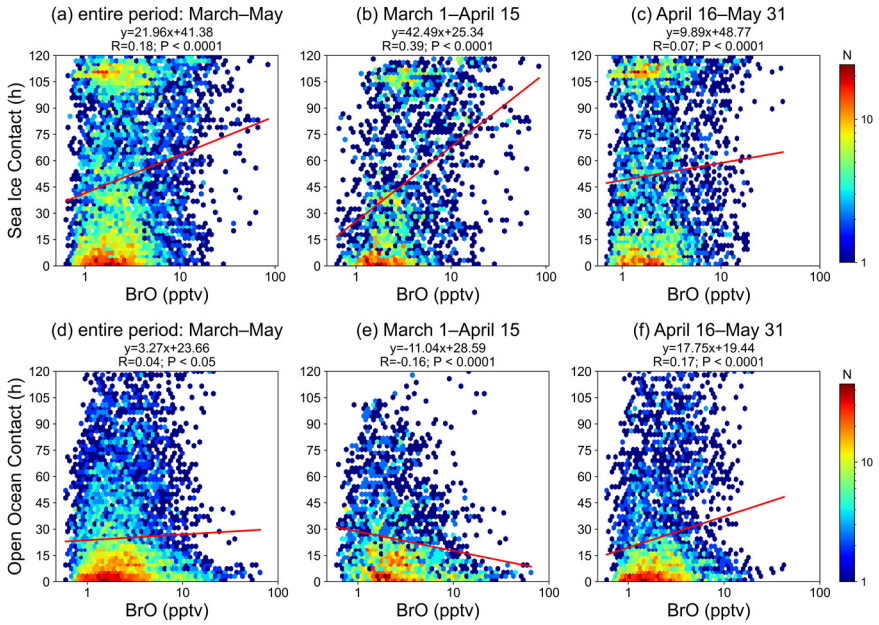

Figure 12. Same as Fig. 10, but for 2019.

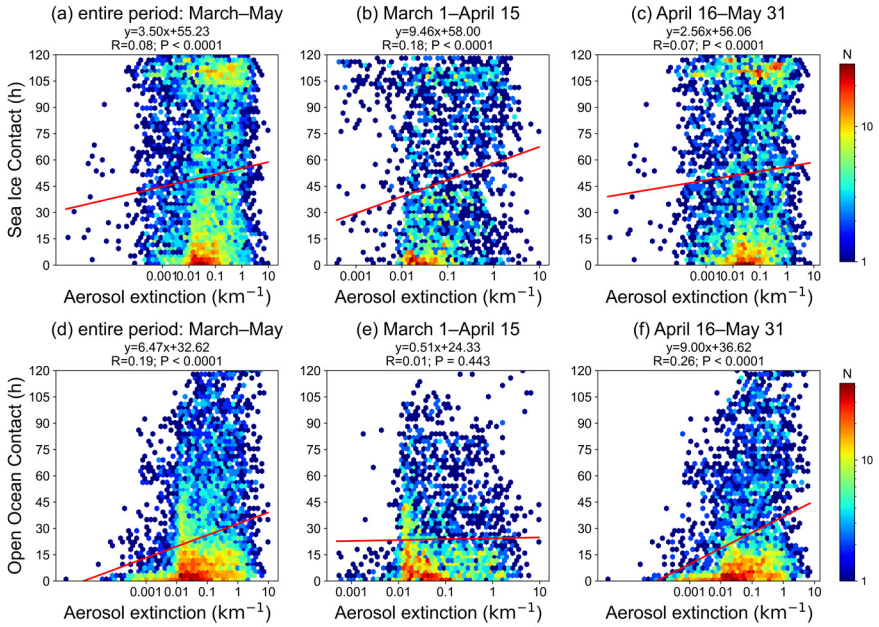

Figure 13. Same as Fig. 11, but for 2019.

Q1.11: Maybe add correlation plots for the vertically integrated quantities (BrO and AOD versus ocean and sea ice contact times).

A1.11: We analyzed correlations for BrO partial columns and AOD, using total sea ice and open ocean contact time summed vertically over 0–3 km, as shown in Figs. 14–17. For both 2019 and 2020, BrO partial columns exhibit stronger positive correlations with total sea ice contact in the first half of the period (March 1–April 15) than in the second half (April 16–May 31), while correlations with total open ocean contact tend to increase in the second half. AOD shows generally weaker correlations and a somewhat different seasonal pattern than BrO. These vertically integrated results are generally consistent with the profiles analysis (Figs. 10–13) and indicate a seasonal shift in the relative influence of sea ice and open ocean contact on BrO and aerosol variability.

The modifications described above have been implemented in the manuscript (P19, lines 473–479).

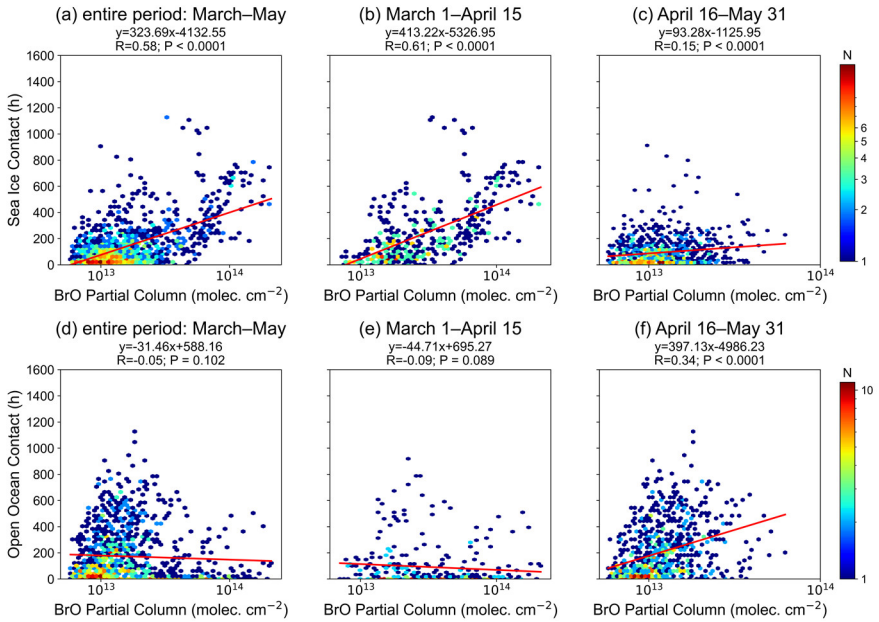

Figure 14. Correlation analysis between BrO partial column and total surface contact time summed over 15 vertical levels (0–3 km) for sea ice and open ocean in 2020. Panels (a–c) show the correlation between BrO partial column and total sea ice contact time: (a) for the entire period from March to May, (b) for the first half of the period (March 1–April 15), and (c) for the second half (April 16–May 31). Panels (d–f) show the correlation between BrO partial column and total open ocean contact time: (d) for the entire period, (e) for the first half, and (f) for the second half.

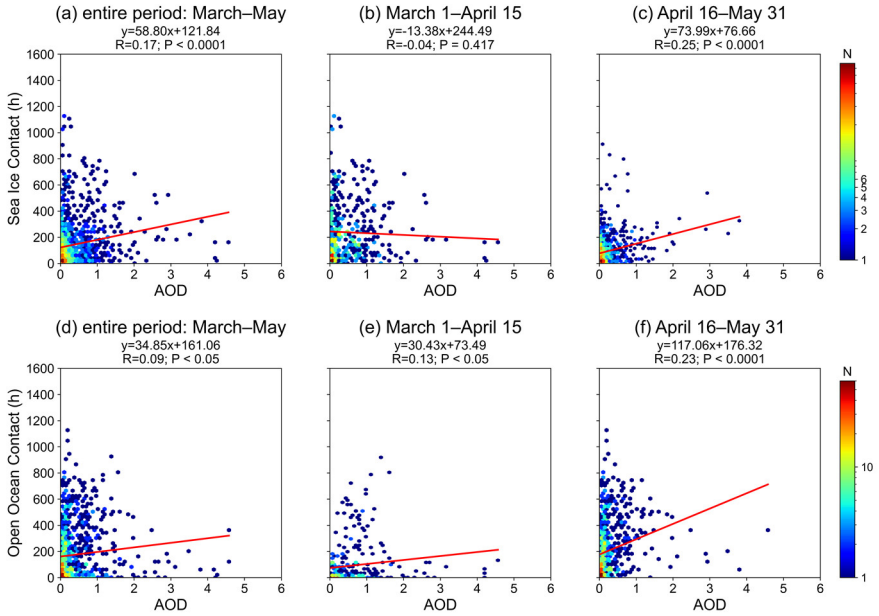

Figure 15. Correlation analysis between AOD and total surface contact time summed over 15 vertical levels (0–3 km) for sea ice and open ocean in 2020. Panels (a–c) show the correlation between AOD and total sea ice contact time: (a) for the entire period from March to May, (b) for the first half of the period (March 1–April 15), and (c) for the second half (April 16–May 31). Panels (d–f) show the correlation between AOD and total open ocean contact time: (d) for the entire period, (e) for the first half, and (f) for the second half.

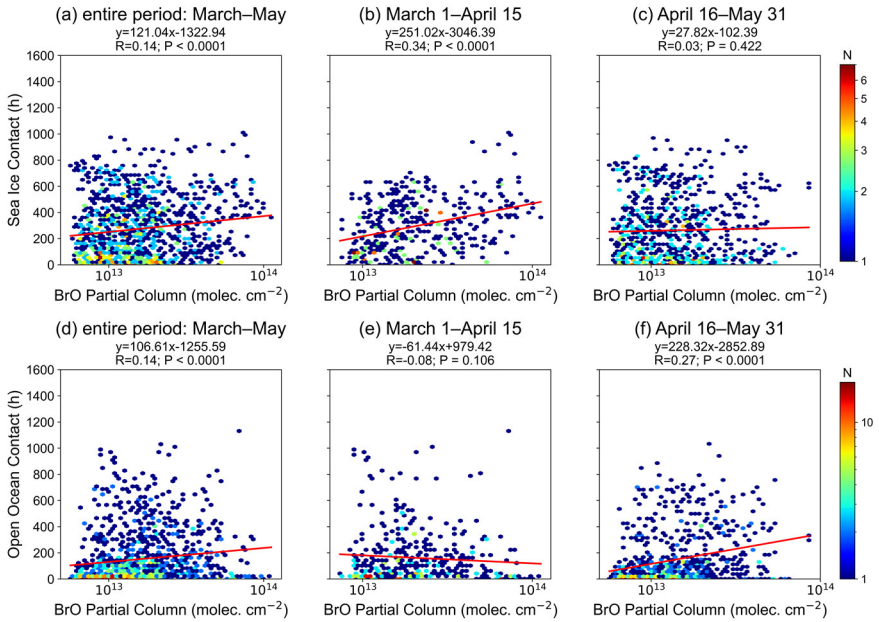

Figure 16. Same as Fig. 14, but for 2019.

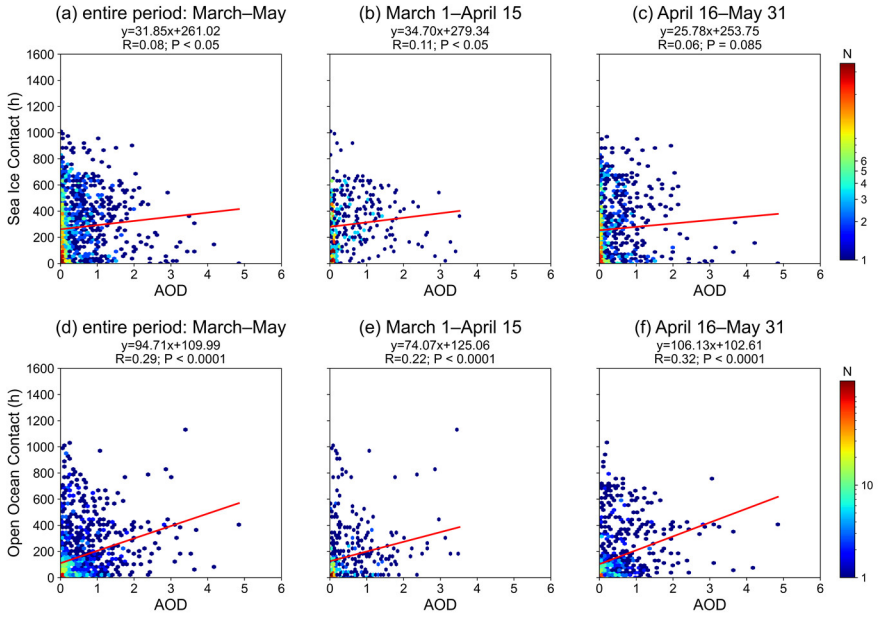

Figure 17. Same as Fig. 15, but for 2019.

Q1.12: Fig. S5: a similar figure for the ocean contact time would be interesting.

A1.12: We analyzed the correlation between BrO VMR (0–3 km) and open ocean contact time for 2017–2023, shown in Fig. 18. Correlations were calculated for all wind speeds, as well as separately for low wind (≤ 7 m s^{-1}) and high wind (> 7 m s^{-1}) conditions. Based on the combined 2017–2023 data, BrO correlations with open ocean contact time are generally weak across March–May, with only minor differences between low and high wind conditions. These results suggest that, unlike the case for sea ice, wind speed does not strongly influence the relationship between BrO and open ocean contact when all years are considered together.

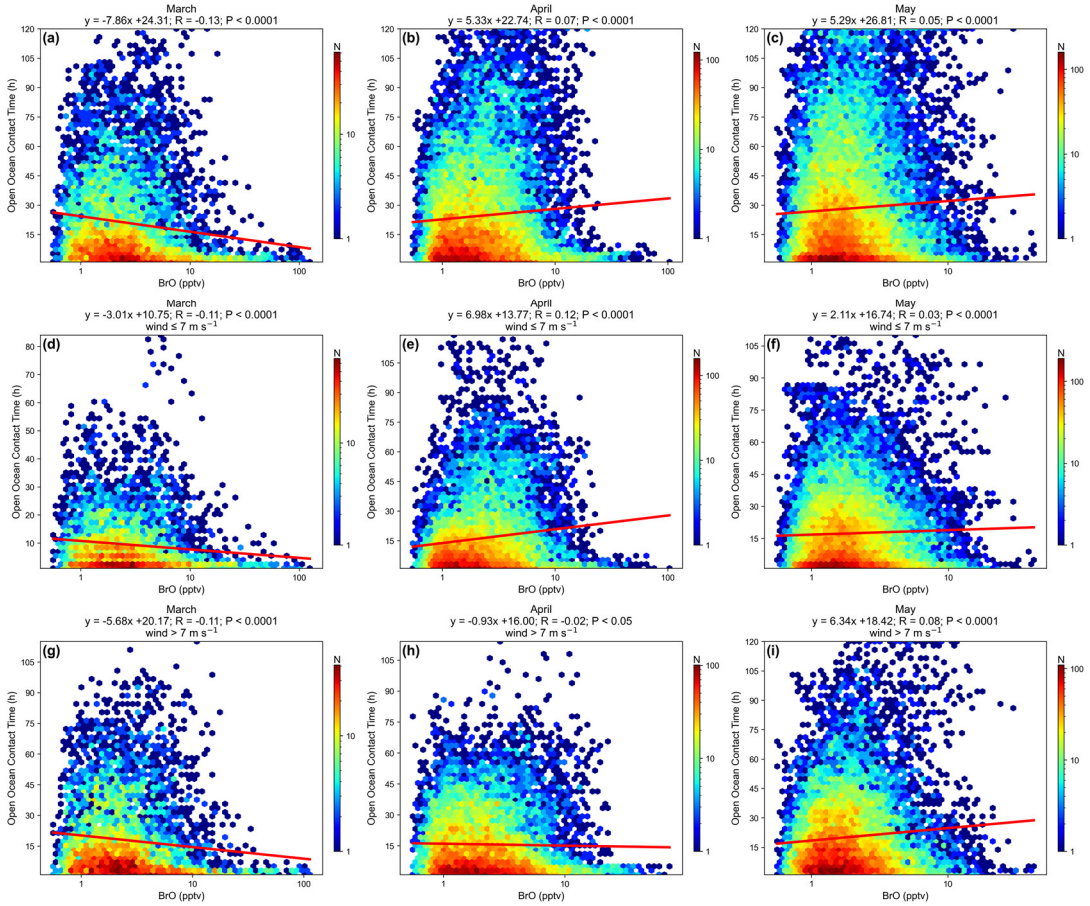

Figure 18. Correlation analysis of BrO VMR (0–3 km altitude) with open ocean contact time from March to May during 2017–2023. (a–c) Correlations between BrO and overall open ocean contact time; (d–f) Correlations between BrO and open ocean contact time during low wind speed conditions (wind ≤ 7 m s^{-1}); (g–i) Correlations between BrO and open ocean contact time during high wind speed conditions (wind > 7 m s^{-1}).

The corresponding section of the manuscript has been modified as below (P30, lines 624–627):

"Based on the combined 2017–2023 data, BrO correlations with open ocean contact time are generally weak across March–May, with only minor differences between low and high wind conditions (Fig. S22). These results suggest that, unlike the case for sea ice, wind speed does not strongly influence the relationship between BrO and open ocean contact when all years are considered together."

Technical corrections:

Q1.13: Fig. 6: add information on the time resolution of the different data sets

A1.13: We have added this information: all data are shown at hourly resolution.

Q1.14: Fig. S1: the y-axes should be labeled ‚BrO partial VCD'

A1.14: We have corrected the y-axis label in Fig. S1 to "BrO partial columns and VCD_{trop} (10^{13}

molec. cm^{-2})”

Q1.15: Fig. S5: add the altitude range of the BrO VMR to the figure caption

A1.15: We have updated the figure caption to include the altitude range: “Correlation analysis of BrO VMR (0–3 km altitude) with sea ice contact time from March to May during 2017–2023.”

Response to Reviewer #2

Reviewer #2 Comments and Suggestions for Authors:
The paper by Li et al. with the title "Tropospheric bromine monoxide in Ny-Ålesund: source analysis and impacts on the atmospheric chemistry" presented a comprehensive dataset, including BrO, ozone, aerosol, and mercury observations and modelled results. Bromine explosion is an old topic, but it still has many unknowns for the atmospheric research community. The paper has good in-depth new findings of both measurements and modelling work. I would support publishing this work if the authors could address my questions and concerns listed here.

Author's Response: We thank Reviewer #2 for the valuable comments, which greatly improve this manuscript. Please kindly find our point-by-point responses to the problems/comments below in blue, and changes to the manuscript in orange.

Major comments:

Q2.1: Line 25-26: This is a misleading claim. Contacting time does not necessarily mean contributions to BEEs. The longer contact with multi-year sea ice only suggests the possibility, but can not be used as a conclusive reason. Multi-year sea ice has lower salinity has been viewed as less possible as a major bromine source. To support this argument, more analysis is needed. E.g., can the increase in BrO signals from GOME be linked to the multi-year ice area? How can we rule out that 23.8% contact with first-year ice is not the real major contributor to the bromine? Some analysis, such as extreme cases, might help. E.g., if you can find any case that is only in contact with multi-year sea ice.

A2.1: We thank the reviewer for this important and constructive comment. We agree that air-mass contact time with a given surface type does not directly quantify its contribution to bromine explosion events (BEEs). We have revised the corresponding sentence to clarify that longer contact with multi-year sea ice (MYI) indicates a potential rather than a conclusive contribution to BEEs. As suggested, a representative BrO enhancement case was added to the revised version to demonstrate the importance of MYI, as shown below.

This BEE, occurring between the afternoon of 1 April 2020 and 3 April 2020 over Ny-Ålesund, was captured by both GOME-2B satellite observations and ground-based MAX-DOAS measurements (Fig. 1, Fig. 2b-d). This BEE was also well captured by p-TOMCAT model (Fig. 1).
To investigate the source regions of this BrO enhancement, we performed analyses for surface meteorological conditions (Fig. 2e-l) and ran 5-day backward trajectories arriving at Ny-Ålesund at 10 m, 200 m, and 500 m altitude, with results shown alongside the sea ice distribution (Fig. 2m-p). As shown, this BEE is associated with an approaching low-pressure system moving from the central Arctic (Fig. 2e-h). Under this system, air masses over the MYI were constrained by Greenland's topography and experienced enhanced surface winds (Fig. 2i-l). Before the low-pressure system approached Ny-Ålesund (ahead of 12:00 1 April), air

masses were mainly from first-year sea ice (FYI) (Fig. 2m-n), where no significant BrO enhancements were measured despite strong winds. However, when air masses passed over the MYI (as shown in Fig. 2o), enhanced BrO was detected. The same case was also reported in Zilker et al. (2023), who performed FLEXPART-WRF backward trajectory analyses of near-surface air masses arriving at Ny-Ålesund on 2 April 2020 at 11:00 UTC. Their 0–50 m backward analysis showed that particles arriving at Ny-Ålesund originated mainly from the northern MYI-covered regions. This suggests that the enhanced BrO observed at Ny-Ålesund is likely related to the transport of reactive bromine associated with sea-salt aerosols produced over MYI.

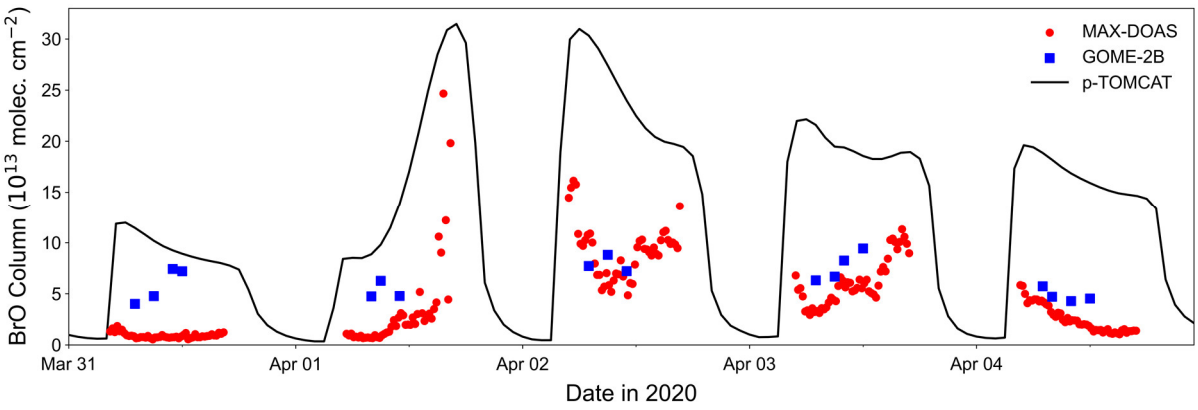

Figure 1. MAX-DOAS BrO partial columns (red scatters), GOME-2B tropospheric BrO columns (blue scatters) and p-TOMCAT BrO partial columns (black line) between 31 March and 4 April in 2020 at Ny-Ålesund.

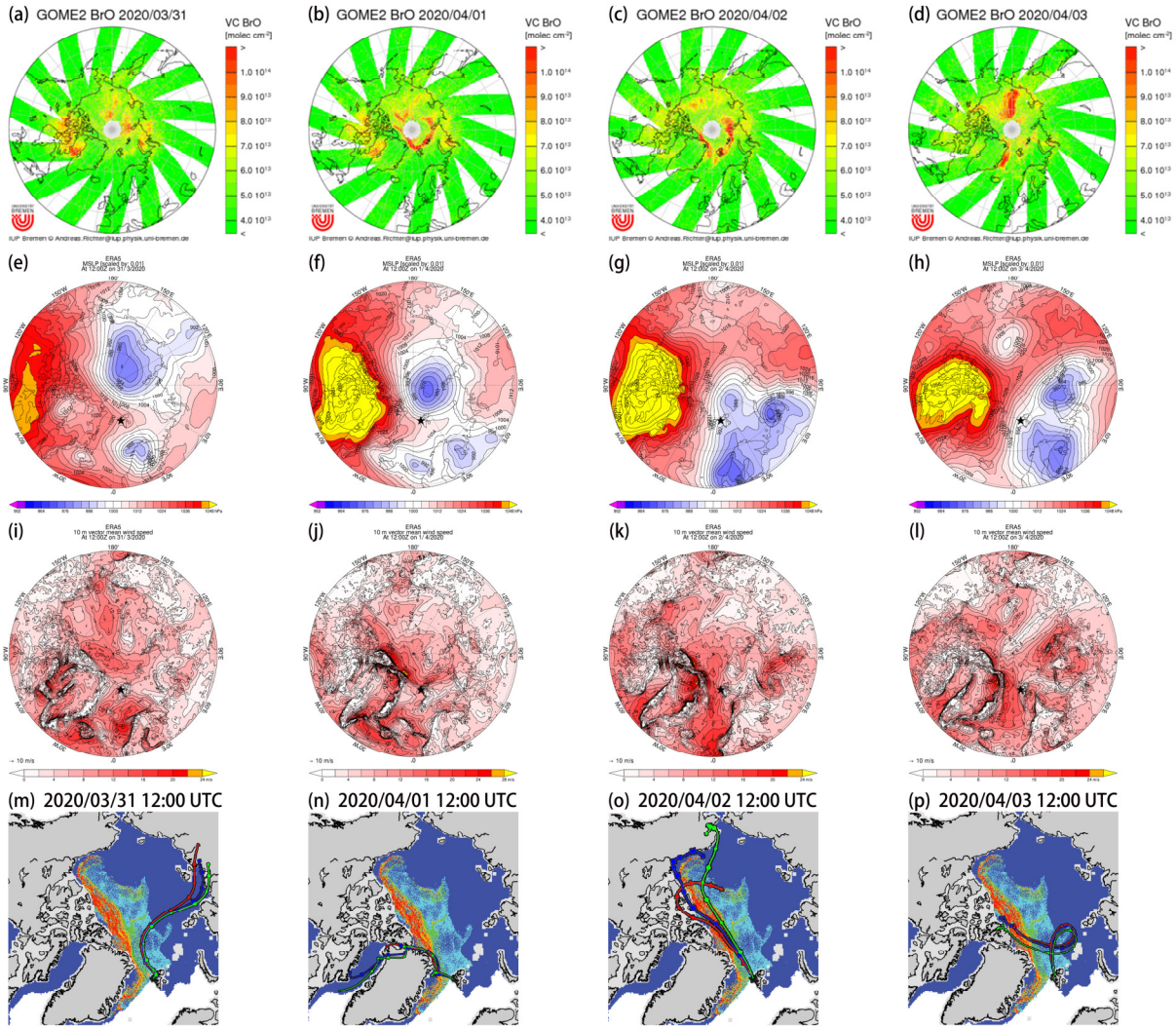

Figure 2. (a, b, c, d) GOME-2B tropospheric BrO columns; (e, f, g, h) Mean sea level pressure; (i, j, k, l) wind speed; (m, n, o, p) Air mass trajectories at 10 m (red line), 200 m (blue line), and 500 m (green line) combined with sea ice, from 31 March 2020, 12:00 UTC to 3 April 2020, 12:00 UTC in Ny-Ålesund.

Furthermore, we derived wind speed distributions over MYI and FYI for all BEEs (2017–2023) based on 5-day backward trajectories. Figure 3 shows that during BEEs, air masses generally take about 2.4 times longer contact time over MYI than over FYI across the full wind-speed range (0–30 m s^{-1}). For wind speeds exceeding 7 m s^{-1}, air masses generally take about 2.8 times longer contact time over MYI (41522 h) than over FYI (14886 h).

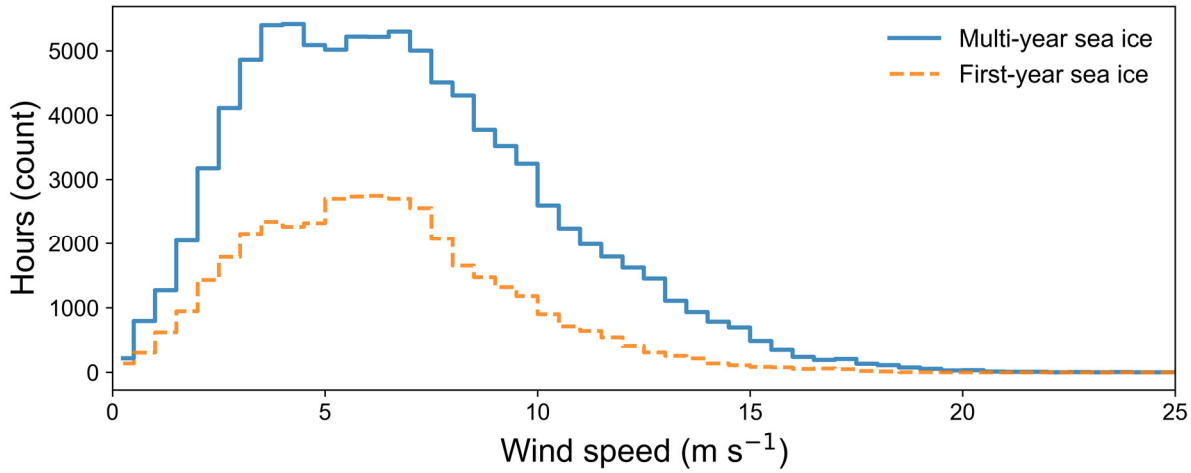

Figure 3. Wind speed distributions along backward trajectories of air masses arriving at Ny-Ålesund during BEEs, separated by trajectory segments over MYI and FYI. The distribution represents combined statistics for March–May during 2017–2023, expressed as the total number of hours in each wind-speed bin.

The corresponding section of the manuscript has been modified as below:

3.5 Potential role of MYI in BEEs

To further investigate the importance of MYI to BEEs, we present a representative case study of BrO enhancement. This BEE, occurring between the afternoon of 1 April 2020 and 3 April 2020 over Ny-Ålesund, was captured by both GOME-2B satellite observations and ground-based MAX-DOAS measurements as well as p-TOMCAT model (Fig. 12, Fig. 13b-d). This BEE event was also well captured by p-TOMCAT model (Fig. 12).

To investigate the source regions of this BrO enhancement, we performed analyses for surface meteorological conditions (Fig. 13e-l) and ran 5-day backward trajectories arriving at Ny-Ålesund at 10 m, 200 m, and 500 m altitude, with results shown alongside the sea ice distribution (Fig. 13m-p). As shown, this BEE is associated with an approaching low-pressure system moving from the central Arctic (Fig. 13e-h). Under this system, air masses over the MYI were constrained by Greenland's topography and experienced enhanced surface winds (Fig. 13i-l). Before the low-pressure system approached Ny-Ålesund (ahead of 12:00 1 April), air masses were mainly from FYI (Fig. 13m-n), where no significant BrO enhancements were measured despite strong winds. However, when air masses passed over the MYI (as shown in Fig. 13o), enhanced BrO was detected. The same case was also reported in Zilker et al. (2023), who performed FLEXPART-WRF backward trajectory analyses of near-surface air masses arriving at Ny-Ålesund on 2 April 2020 at 11:00 UTC. Their 0–50 m backward analysis showed that particles arriving at Ny-Ålesund originated mainly from the northern MYI-covered regions. This suggests that the enhanced BrO observed at Ny-Ålesund is likely related to the transport of reactive bromine associated with sea-salt aerosols produced over MYI.

Furthermore, we derived wind speed distributions over MYI and FYI for all BEEs (2017–2023) based on 5-day backward trajectories. Figure 14 shows that during BEEs, air masses generally take about 2.4 times longer contact time over MYI than over FYI across the full wind-speed range (0–30 m s^{-1}). For wind speeds exceeding 7 m s^{-1}, air masses generally take about 2.8

times longer contact time over MYI (41522 h) than over FYI (14886 h).

Zilker, B., Richter, A., Blechschmidt, A.-M., von der Gathen, P., Bougoudis, I., Seo, S., Bösch, T., and Burrows, J. P.: Investigation of meteorological conditions and BrO during ozone depletion events in Ny-Ålesund between 2010 and 2021, Atmos. Chem. Phys., 23, 9787–9814, https://doi.org/10.5194/acp-23-9787-2023, 2023.

Q2.2: Line 57-59: since your major finding is that multi-year sea ice plays important role than first-year sea ice, more descriptions of current understandings and previous findings on these two sources should be provided. What are the differences between first and multi-year sea ice in terms of bromine chemistry? If they are both considered as sources, are they considered on a similar or different level in the BEE contributions?

A2.2: We added a new paragraph in the Introduction Part (shown below) to summarise our current understanding and previous findings regarding FYI and MYI as potential bromine sources.

"FYI and MYI differ in their physical and chemical properties, which may influence the efficiency of bromine activation. MYI is generally thicker and less porous than FYI, and these physical characteristics limit brine connectivity within the ice and its upward transport, resulting in distinct roles in Arctic bromine chemistry (Haas et al., 2006, 2010). After undergoing multiple summer melt–refreeze cycles, MYI is desalinated through gravity drainage and flushing, whereas FYI typically retains higher salinity (Krnavek et al., 2012). Although brine can migrate upward through the ice–snow interface and supply salts to overlying snow, this process is highly sensitive to snow depth, with observations suggesting an effective upper limit of approximately 17 cm (Domine et al., 2004). MYI regions generally accumulate deeper snowpacks, limiting the upward transport of salts from the ice and resulting in lower snow salinity compared to FYI (Webster et al., 2014; Blanchard-Wrigglesworth et al., 2015). Under such low-salinity conditions, atmospheric deposition and recycling may become increasingly important in controlling bromide availability in the snow (Krnavek et al., 2012; Nandan et al., 2017). Surface snow over MYI typically exhibits low salinity, with typical median value around 0.01 practical salinity unit (psu), whereas snow over FYI is generally more saline, with median values ranging from 0.1 to 0.7 psu (Krnavek et al., 2012). Analysis of bromine enrichment factors indicates that bromide depletion is more frequently observed in snow over MYI compared to snow over FYI, suggesting that, in addition to FYI, MYI may actively participate in Arctic boundary layer bromine chemistry (Peterson et al., 2019). This explains the enhanced tropospheric BrO observed over MYI regions (Peterson et al., 2016; Burd et al., 2017). Further modeling studies suggest that blowing-snow–sourced sea-salt aerosol emissions from MYI regions may contribute approximately 20–30% of Arctic springtime tropospheric BrO enhancement, indicating that MYI represents a significant source of bromine activation (Huang et al., 2020). A recent field measurement in the high Arctic coastal area (Yang et al., 2024) provide evidence for the dominant role of atmospheric processes in controlling surface-layer bromide concentrations. For example, snow samples collected from offshore and onshore sites during early springtime at Eureka, Canada, show

very low salinities in the snow skin layer (<1 cm), with corresponding bromide enriched by up to a factor of 10, suggesting the importance of atmospheric deposition processes. As a result, they could serve as a direct source of reactive bromine once lifted by winds, even though the corresponding salinity is very low. Current chemistry models do not take this effect into account."

Blanchard-Wrigglesworth, E., Farrell, S. L., Newman, T., and Bitz, C. M.: Snow cover on Arctic sea ice in observations and an Earth System Model, Geophys. Res. Lett., 42, 10,342–10,348, https://doi.org/10.1002/2015GL066049, 2015.

Burd, J. A., Peterson, P. K., Nghiem, S. V., Perovich, D. K., and Simpson, W. R.: Snowmelt onset hinders bromine monoxide heterogeneous recycling in the Arctic, J. Geophys. Res. Atmos., 122, 8297–8309, https://doi.org/10.1002/2017JD026906, 2017.

Domine, F., Sparapani, R., Ianniello, A., and Beine, H. J.: The origin of sea salt in snow on Arctic sea ice and in coastal regions, Atmos. Chem. Phys., 4, 2259–2271, https://doi.org/10.5194/acp-4-2259-2004, 2004.

Haas, C., Hendricks, S., and Doble, M.: Comparison of the sea-ice thickness distribution in the Lincoln Sea and adjacent Arctic Ocean in 2004 and 2005, Ann. Glaciol., 44, 247–252, https://doi.org/10.3189/172756406781811781, 2006.

Haas, C., Hendricks, S., Eicken, H., and Herber, A.: Synoptic airborne thickness surveys reveal state of Arctic sea ice cover, Geophys. Res. Lett., 37, L09501, https://doi.org/10.1029/2010GL042652, 2010.

Huang, J., Jaeglé, L., Chen, Q., Alexander, B., Sherwen, T., Evans, M. J., Theys, N., and Choi, S.: Evaluating the impact of blowing-snow sea salt aerosol on springtime BrO and O3 in the Arctic, Atmospheric Chemistry and Physics, 20, 7335–7358, https://doi.org/10.5194/acp-20-7335-2020, 2020.

Krnavek, L., Simpson, W. R., Carlson, D., Domine, F., Douglas, T. A., and Sturm, M.: The chemical composition of surface snow in the Arctic: Examining marine, terrestrial, and atmospheric influences, Atmos. Environ., 50, 349–359, https://doi.org/10.1016/j.atmosenv.2011.11.033, 2012.

Nandan, V., Geldsetzer, T., Yackel, J., Mahmud, M., Scharien, R., Howell, S., King, J., Ricker, R., and Else, B.: Effect of Snow Salinity on CryoSat-2 Arctic First-Year Sea Ice Freeboard Measurements, Geophys. Res. Lett., 44, 10419–10426, https://doi.org/10.1002/2017GL074506, 2017.

Peterson, P. K., Simpson, W. R., and Nghiem, S. V.: Variability of bromine monoxide at Barrow, Alaska, over four halogen activation (March–May) seasons and at two on-ice locations, J. Geophys. Res. Atmos., 121, 1381–1396, https://doi.org/10.1002/2015JD024094, 2016.

Peterson, P. K., Hartwig, M., May, N.W., Schwartz, E., Rigor, I., Ermold, W., Steele, M., Morison, J. H., Nghiem, S. V., and Pratt, K. A.: Snowpack measurements suggest role for multi-year sea ice regions in Arctic atmospheric bromine and chlorine chemistry, Elem. Sci. Anth., 7, 14, https://doi.org/10.1525/elementa.352, 2019.

Webster, M. A., Rigor, I. G., Nghiem, S. V., Kurtz, N. T., Farrell, S. L., Perovich, D. K., and Sturm, M.: Interdecadal changes in snow depth on Arctic sea ice, J. Geophys. Res. Oceans., 119, 5395–5406, https://doi.org/10.1002/2014JC009985, 2014.

Yang, X., Strong, K., Criscitiello, A. S., Santos-Garcia, M., Bognar, K., Zhao, X., Fogal, P.,

Walker, K. A., Morris, S. M., and Effertz, P.: Surface snow bromide and nitrate at Eureka, Canada, in early spring and implications for polar boundary layer chemistry, Atmos. Chem. Phys., 24, 5863–5886, https://doi.org/10.5194/acp-24-5863-2024, 2024.

In this study, snow salinity over FYI is based on MOSAiC measurements (Macfarlane et al., 2023); over MYI, half the FYI salinity is applied, which accounts for the two opposing effects: lower snow salinity but higher bromine enrichment. As shown in Figure 4, the calculated blowing-snow-sourced bromine emissions during 2017-2023 BEEs indicate that bromine flux over MYI accounts for an average of 54% (35–67%) of total bromine flux over sea ice.

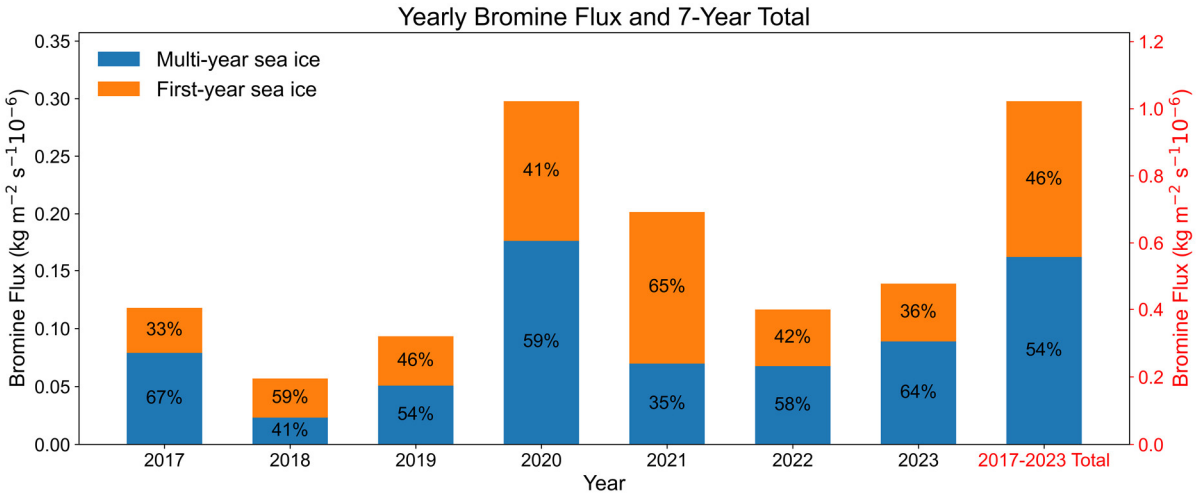

Figure 4. Yearly (March–May) and seven-year total blowing-snow-sourced bromine emission fluxes over MYI and FYI along backward trajectories of air masses arriving at Ny-Ålesund during BEEs. Blue and orange bars indicate the contributions from MYI and FYI, respectively.

The corresponding section of the manuscript has been modified as below:

"Snow salinity values over FYI used in the study were obtained from the MOSAiC measurements (Macfarlane et al., 2023); over MYI, half the FYI salinity is applied, which accounts for the two opposing effects: lower snow salinity but higher bromine enrichment. As shown in Figure S2, the calculated blowing-snow-sourced bromine emissions during 2017-2023 BEEs indicate that bromine flux over MYI accounts for an average of 54% (35–67%) of total bromine flux over sea ice."

Macfarlane, AR, Schneebeli, M, Dadic, R, Tavri, A, Immerz, A, Polashenski, C, Krampe, D, Clem ens-Sewall, D, Wagner, DN, Perovich, DK, Henna-Reetta, H, Raphael, I, Matero, I, Regnery, J, Smith, MM, Nicolaus, M, Jaggi, M, Oggier, M, Webster, MA, Lehning, M, Kolabutin, N, Itkin, P, Naderpour, R, Pirazzini, R, Ha¨mmerle, S, Arndt, S, Fons, S.: A database of snow on sea ice in the central Arctic collected during the MOSAiC expedition. Scientific Data, 10, 398, http:// dx.doi.org/10.1038/s41597-023-02273-1, 2023.

Q2.3: Line 118-124: I understand this is a complicated research topic and the background is rich. The author did a good job of providing some background. However, I still read that the

introduction part is not well organized. E.g., the author talked about the general features of studies of BEE first, then discussed the local observations from Ny-Ålesund. In this part, they go back to the other field findings again.

A2.3: We have reorganized the structure of the introduction accordingly, e.g. by moving the section on local observations from Ny-Ålesund to the penultimate paragraph. The new introduction flow from the general background on BEE to the specific local context.

Q2.4: Line 178: In March, I would expect the site still to have snow cover. Can the author explain why surface albedo is set to only 0.1? Even in the referenced paper, this 0.1 surface albedo is not specifically discussed. But, for satellite, typically 0.9 will be used for such conditions. Comments?

A2.4: Thank you for the comment. We note that in March, although the site itself may be snow-covered, the surrounding ocean is presented by open seawater due to the influence of the North Atlantic Warm Current.

For our ground-based MAX-DOAS analysis, we used the SCIATRAN software (Rozanov et al., 2005) to get the modeled differential Air Mass Factor (DAMF) at 2° elevation based on assumed BrO profiles with air masses distributed between 0–4 km, corresponding to the a priori profiles used in the profile retrievals. Figure 5 shows the modeled DAMF at 2° elevation at Ny-Ålesund in March as a function of solar zenith angle (SZA) under different surface albedo conditions. It can be seen that the DAMF does not change significantly with different surface albedo, with an average difference of approximately 1.8% between surface albedo values of 0.1 and 0.9. This is consistent with Wagner et al. (2007), who reported that, in contrast to satellite observations, ground-based MAX-DOAS sensitivity is almost independent of the surface albedo and hardly decreases at large SZAs. Therefore, using a surface albedo of 0.1 in our simulations has a negligible effect on the resulting DAMFs.

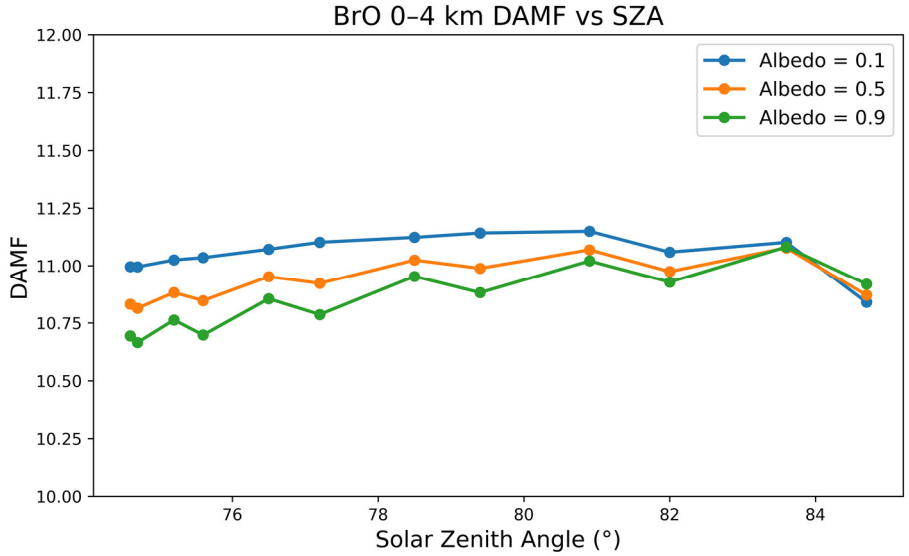

Figure 5. Modeled MAX-DOAS DAMF at 2° elevation at Ny-Ålesund in March as a function of SZA under different surface albedos (0.1, 0.5, 0.9).

The corresponding section of the manuscript has been modified as below:

"The surface albedo was set to 0.1 (Chen et al., 2022). In contrast to satellite observations, MAX-DOAS sensitivity is almost independent of the surface albedo and hardly decreases at large SZAs (Wagner et al., 2007)."

Chen, D., Luo, Y., Yang, X., Si, F., Dou, K., Zhou, H., Qian, Y., Hu, C., Liu, J., and Liu, W.: Study of an Arctic blowing snow-induced bromine explosion event in Ny-Alesund, Svalbard, Sci Total Environ, 839, 156335, https://doi.org/10.1016/j.scitotenv.2022.156335, 2022.

Rozanov, A., Bovensmann, H., Bracher, A., Hrechanyy, S., Rozanov, V., Sinnhuber, B.-M., Stroh, F., and Burrows, J. P.: NO_2 and BrO vertical profile retrieval from SCIAMACHY limb measurements: Sensitivity studies, Adv. Space Res., 36, 846–854, https://doi.org/10.1016/j.asr.2005.03.013, 2005.

Wagner, T., Ibrahim, O., Sinreich, R., Frieß, U., von Glasow, R., and Platt, U.: Enhanced tropospheric BrO over Antarctic sea ice in mid winter observed by MAX-DOAS on board the research vessel Polarstern, Atmos. Chem. Phys., 7, 3129–3142, https://doi.org/10.5194/acp-7-3129-2007, 2007.

Q2.5: Line 219-220: p-TOMCAT is driven by ERA5, while HYSPLIT is driven by GDAS. These datasets have different vertical, horizontal, and even temporal resolutions (6 hr vs. 1 hr). Any comments on the impact of different meteorological inputs? Since p-TOMCAT is a transport model, is it possible to directly analyze sea-ice contact information from p-TOMCAT simulations?

Line 263-268: Isn't such emission flux information part of the p-TOMCAT simulation results? If yes, what does it look like? If not, what are the main challenges here? Anyway, the point is that hybridizing results from a transport model with another trajectory model seems redundant and questionable (mainly, they are driven by different meteorological fields that have very different resolutions).

A2.5: The above two questions will be answered together here. Note that p-TOMCAT uses ERA5-based reanalysis data, while HYSPLIT uses GDAS data. In p-TOMCAT, the 6-hourly ERA5 meteorological fields at their native resolution (0.25° × 0.25°) are regridded to a coarse horizontal resolution of 2.825° × 2.825° for use in the simulations. The p-TOMCAT output is archived at hourly intervals. GDAS provides 1° × 1° analyses every 6 hours, and HYSPLIT outputs hourly trajectories at 1° × 1° resolution.

Regarding the impact of different meteorological inputs, we acknowledge that differences in temporal and spatial resolution may affect the resulting transport and derived quantities. To investigate this, we compared bromine fluxes calculated from blowing snow along 5-day backward trajectories (1° × 1°), using the corresponding ERA5 meteorological data (0.25° × 0.25°, hourly) with the same parameterization as in the model, and with those obtained directly from p-TOMCAT's outputs. Figure 6 shows that bromine fluxes calculated directly from ERA5 data are approximately 2.8 times larger than those from p-TOMCAT for the period of March–

May 2020. The elevated flux in the ERA5 calculation is largely attributed to the high meteorological resolution, while the coarse model horizontal resolution may smooth out sub-grid meteorological variability. In addition, p-TOMCAT does not distinguish between MYI and FYI; areas where sea ice persisted through the preceding summer are treated as MYI, which contributes to the bias. For this reason, rather than taking the values directly from the model's outputs, we combined HYSPLIT backward trajectories with ERA5 meteorology and incorporated higher-resolution sea-ice conditions to directly derive bromine emission fluxes, which is essential for diagnosing spatially localized bromine emission fluxes.

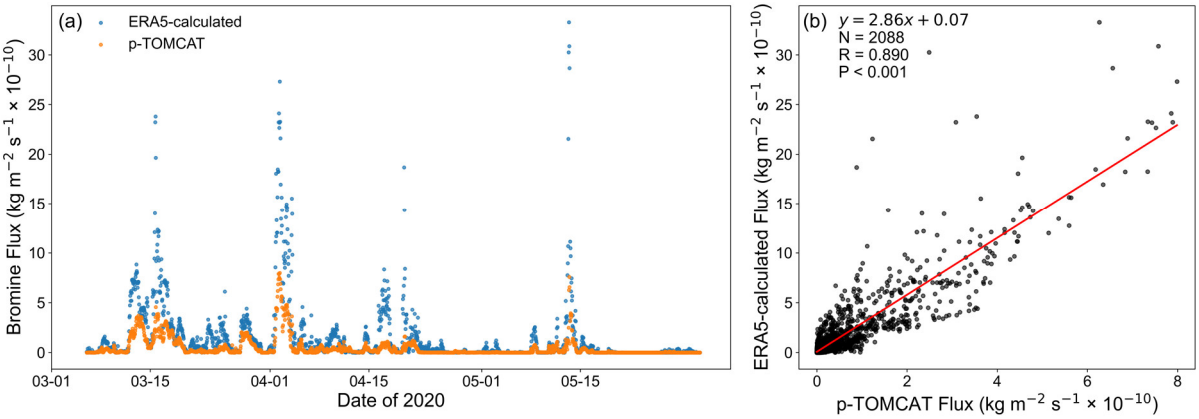

Figure 6. (a) Time series of blowing-snow-sourced bromine fluxes calculated from ERA5 meteorological fields (blue dots) and from the p-TOMCAT (orange dots) during March–May 2020. The fluxes are summed over the 0–3 km layer and shown at hourly resolution. (b) Scatter plot showing the correlation between the ERA5-calculated and p-TOMCAT-simulated blowing-snow-sourced bromine fluxes over the same period.

The corresponding section of the manuscript has been modified as below:

"In our simulations, ERA5 fields at their native horizontal resolution (0.25° × 0.25°) were first regridded to match the p-TOMCAT horizontal resolution (2.825° × 2.825°)."

"These bromine emission fluxes are not taken directly from p-TOMCAT model output; instead, they are calculated using native-resolution ERA5 meteorology along backward trajectories. In addition to p-TOMCAT's coarse horizontal resolution, monthly sea-ice coverage (Rayner et al., 2003) was used without distinguishing between MYI and FYI; areas where sea ice persisted through the preceding summer are therefore treated as MYI in a coarse approximation. As a result, p-TOMCAT cannot precisely distinguish fluxes between MYI and FYI, so the bromine emission fluxes are calculated using ERA5 meteorology. The comparison shows that blowing-snow-sourced bromine fluxes calculated directly from ERA5 can be 2–3 times larger than those from p-TOMCAT outputs, which is likely due to differences in meteorological resolution and sea-ice representation (see Figure S3 in the Supplement)."

Rayner, N. A., Parker, D. E., Horton, E. B., Folland, C. K., Alexander, L. V., Rowell, D. P., Kent, E. C., and Kaplan, A.: Global analyses of sea surface temperature, sea ice, and night marine air temperature since the late nineteenth century, Journal of Geophysical Research: Atmospheres, 108, 4407, https://doi.org/10.1029/2002jd002670, 2003.

Yang, X., Pyle, J. A., and Cox, R. A.: Sea salt aerosol production and bromine release: Role of snow on sea ice, Geophys. Res. Lett., 35, L16815, https://doi.org/10.1029/2008gl034536, 2008.

Q2.6: Figure 5: The general n-shape curve for the number of profiles in Fig 5a and 5c is reasonable. But why Fig 5e show double peaks?

A2.6: The double-peak structure mainly arises from the combined effects of the seasonal evolution of the SZA sampling range and the temporal variation of SZA, as illustrated by the following analysis. Figure 7 shows the SZA distributions corresponding to the actual MAX-DOAS observation times. When all observation times are considered, the SZA distributions in March and April exhibit a single peak, whereas May clearly shows a double-peak structure. This difference is closely related to the seasonal evolution of sunlight conditions in spring. Specifically, the observable SZA range gradually expands over the course of each month: in early March, SZA is mostly within 84–86°, extending to 74–86° by late March; in early April, it spans 74–86°, further extending to 64–86° by late April; while in May, the SZA range exhibits approximately 62–86° in early May and 56–80° in late May. As a result, in May, the distribution of observation time points across SZA is no longer concentrated in a single range but forms two relatively distinct intervals.

Figure 8 highlights how SZA variation rates contribute to the double-peak structure. For example, during morning observations in May, the two SZA intervals around 78–80° and 62–64° correspond to the peaks. The first reason is that observations from both early and late May cover these two intervals, providing sufficient data points in each. The second reason, as shown in Figure 8c, is that SZA changes relatively slowly within these intervals, allowing the instrument to remain longer and accumulate more valid observations. Together, these factors lead to the double peaks in the statistical distribution.

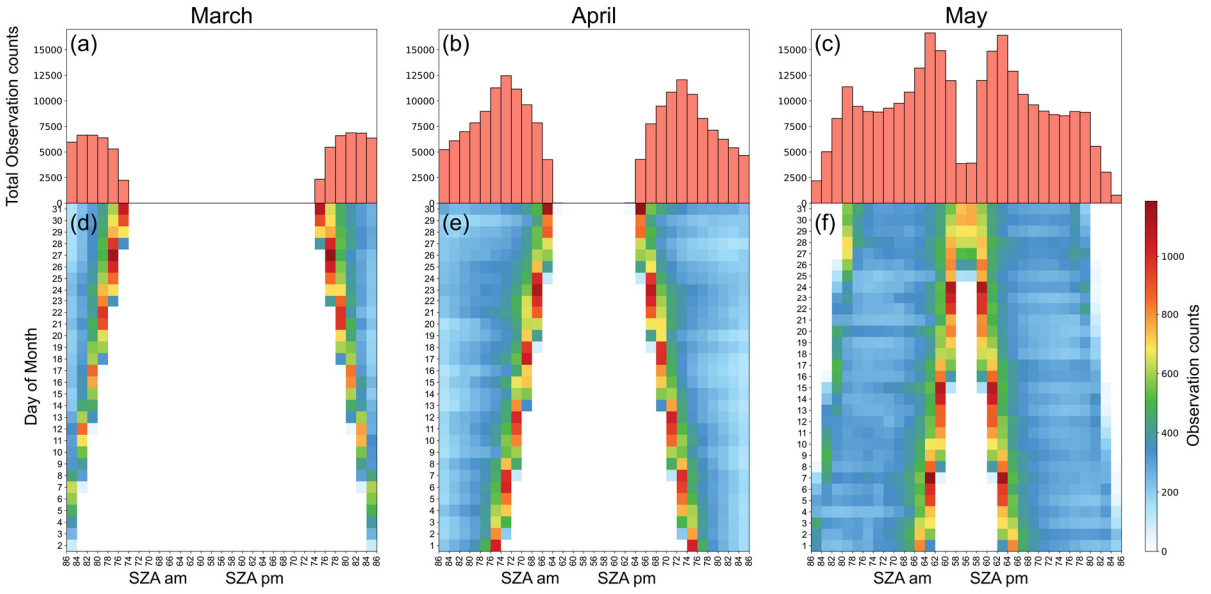

Figure 7. SZA distributions sampled at the times of MAX-DOAS measurements during March (a, d), April (b, e), and May (c, f) in 2017–2023. Panels (a–c) show the total number of observations aggregated across all years as a function of SZA for

morning (AM) and afternoon (PM) conditions, while panels (d–f) present the corresponding daily SZA frequency distributions. March and April are characterized by a single peak at large SZA, whereas May exhibits clear double peaks.

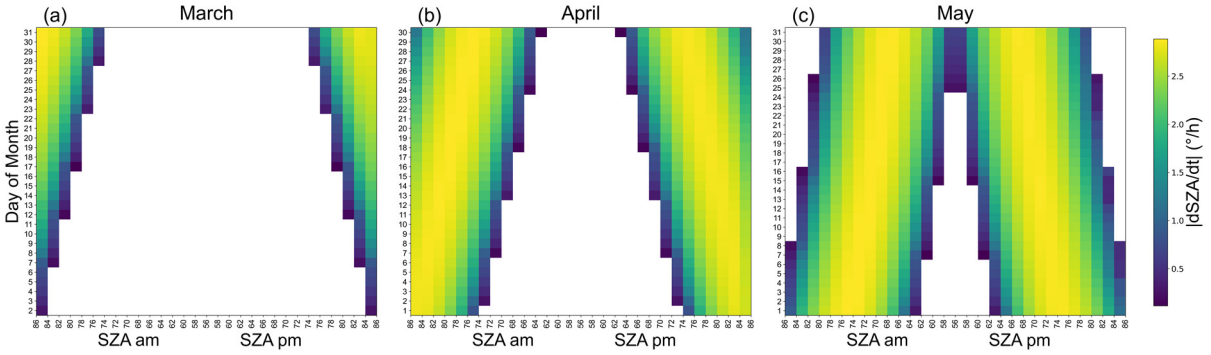

Figure 8. Absolute SZA variation rates (|dSZA/dt|, °/h) sampled at the times of MAX-DOAS measurements in March (a), April (b), and May (c) during 2017–2023. For each day, morning (AM) and afternoon (PM) observations are binned by SZA. Different colors represent the value of |dSZA/dt|, with lower values corresponding to slower SZA variation and higher values to faster SZA variation.

The corresponding section of the manuscript has been modified as below:

"In addition, The double-peak structure (Fig. 5e) in May mainly arises from the seasonal expansion of the observable SZA range and the slower SZA variation at specific SZA intervals, which leads to enhanced sampling at two distinct SZA ranges (78°–80° and 62°–64°; see Figs. S4 and S5)."

Q2.7: Line 368-369: Does this "sea ice contacting time" include both multi-year and first-year sea ice? Please make this clear. Also, if yes, can you break down the sea ice contact time into multi-year and first-year sea ice?

Figures 6 and 7: as the author claimed in the abstract and conclusion that one key finding is that multi-year sea ice plays a key role, I would expect the panels to have "sea ice contact time," meaning the contact with multi-year sea ice (not just all types of sea ice). Please make this clear in the captions and the related discussion part.

A2.7: The above two questions will be answered together here. In the original manuscript (Lines 368–369), the term "sea ice contact time" referred to the total sea ice contact time, including both MYI and FYI. We have now clarified this in the revised manuscript.

Specifically, the back-trajectory-based analysis shows that BrO is significantly positively correlated with total sea ice contact time ($r = 0.48$, $p < 0.0001$), whereas no significant correlation is found with open ocean contact time ($r = -0.02$, $p = 0.145$). Additionally, we find that BrO also exhibits a positive correlation with MYI contact time ($r = 0.47$, $p < 0.0001$), and a weaker but still statistically significant correlation with FYI contact time ($r = 0.22$, $p < 0.0001$).

In response, we have revised the figures and captions to clearly distinguish between total sea ice, MYI, and FYI contact times. The Figures 6 and 7 in the original manuscript have been updated and are now presented as Figures 9 and 10 in this response.

In addition, we have revised the corresponding description in the main text.

"BrO and aerosol extinction profiles, MYI, FYI, total sea ice, and open ocean contact along air mass history trajectories, surface ozone, gaseous mercury, BrO partial column, and key meteorological parameters are presented in Fig. 6."

"Moving to the back-trajectory-based analysis, BrO shows a significant positive correlation with total sea ice contact time (including both MYI and FYI; $r = 0.48$, $p < 0.0001$), whereas no significant correlation is found with open ocean contact time ($r = -0.02$, $p = 0.145$). When separated by ice type, BrO exhibits a statistically significant positive correlation with MYI contact time ($r = 0.47$, $p < 0.0001$), stronger than its correlation with FYI ($r = 0.22$, $p < 0.0001$)."

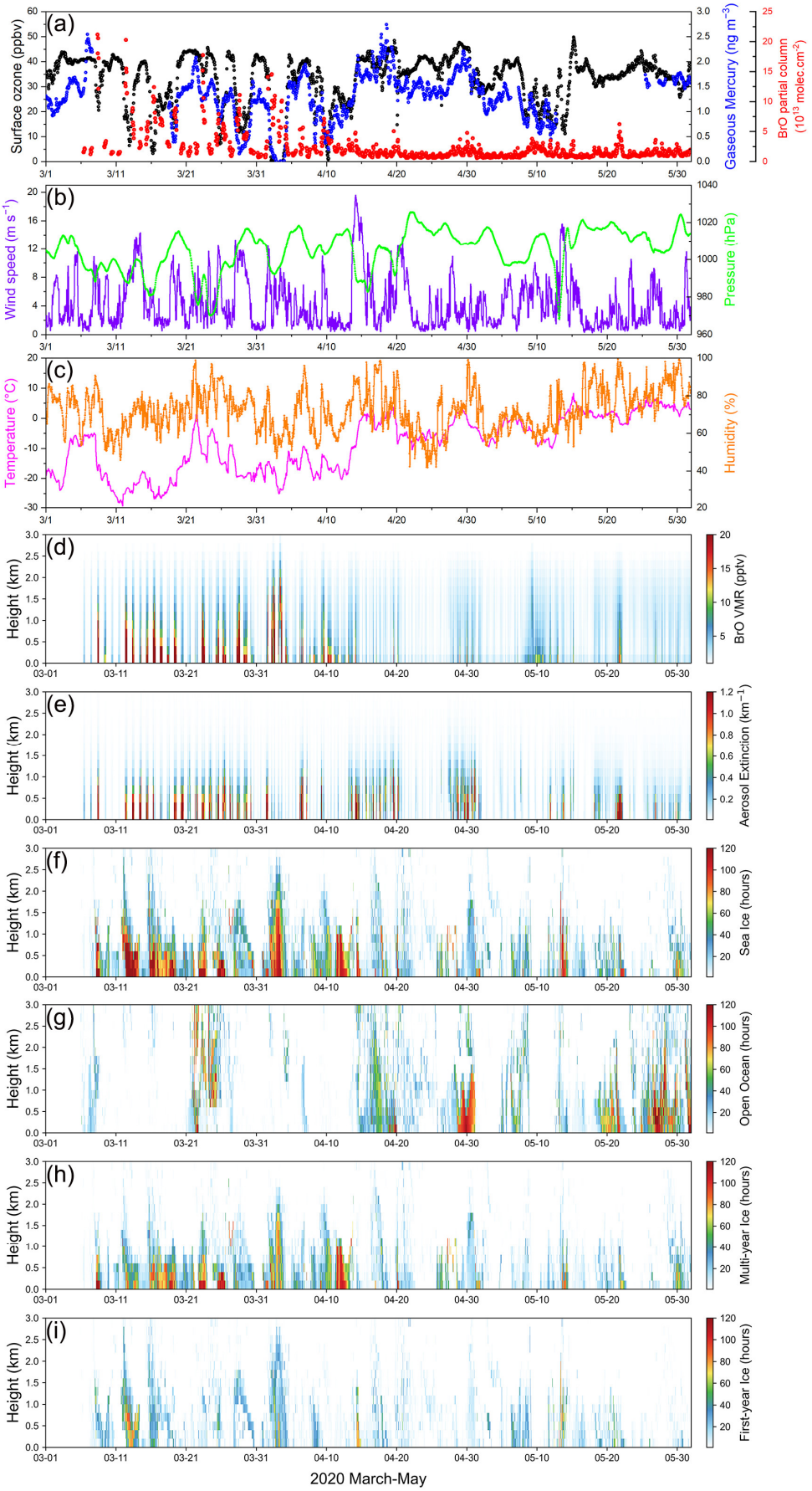
(a)
Surface ozone (ppbv)
Gaseous Mercury (ng m^{-3})
BrO partial column (10^{13} molec.cm^{-2})
(b)
Wind speed (m s^{-1})
Pressure (hPa)
(c)
Temperature (°C)
Humidity (%)
(d)
Height (km)
BrO VMR (pptv)
(e)
Aerosol Extinction (km^{-1})
(f)
Sea Ice (hours)
(g)
Open Ocean (hours)
(h)
Multi-year Ice (hours)
(i)
First-year Ice (hours)
3/1
3/11
3/21
3/31
4/10
4/20
4/30
5/10
5/20
5/30
03-01
03-11
03-21
03-31
04-10
04-20
04-30
05-10
05-20
05-30
2020 March-May

Figure 9. Panel (a) surface ozone (black dots), gaseous mercury (Hg(0)) (blue dots) and BrO partial column (red dots); (b) wind speed (purple line), pressure (green line); (c) temperature (pink line), relative humidity (orange line); (d) BrO profiles; (e) aerosol extinction profiles; (f) total sea ice contact time profiles; (g) open ocean contact time profiles; (h) MYI contact time profiles; and (i) FYI contact time profiles between March and May 2020 in Ny-Ålesund. All data are shown at hourly resolution.

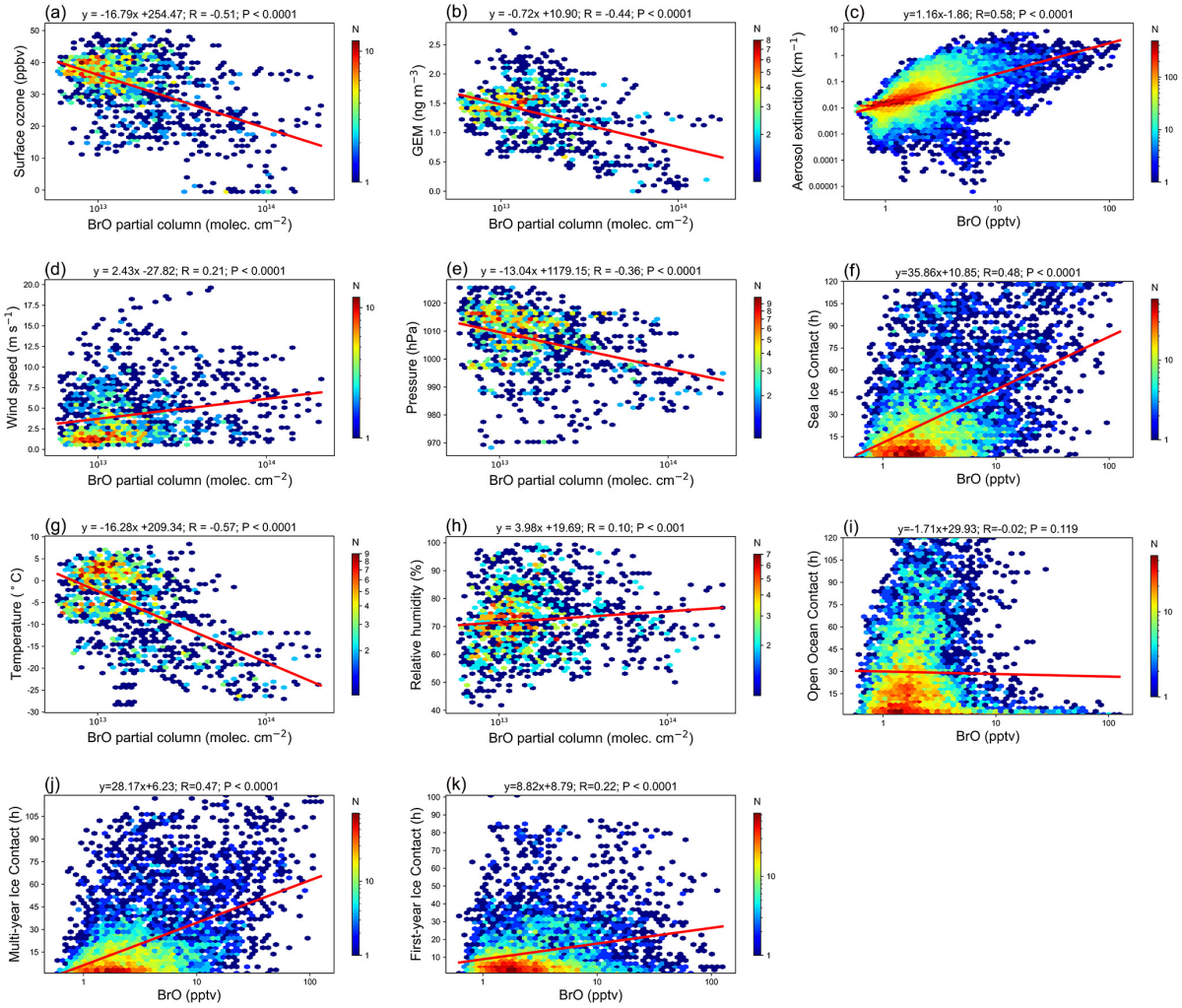

Figure 10. Correlation analysis between BrO and various parameters during March–May 2020. BrO partial column correlations are shown for surface ozone (a), GEM (b), wind speed (d), pressure (e), temperature (g), and relative humidity (h). BrO VMR profile correlations are shown for aerosol profiles (c), total sea ice contact time (f), open ocean contact time (i), MYI contact time (j), and FYI contact time (k).

Q2.8: Line 430-436 and 492-495: My understanding is that the BEE in p-TOMCAT is mainly driven by this SSA production mechanism. But, here it seems the author also wants to emphasize the role of multi-year sea ice. What kind of role does the multi-year sea ice play in p-TOMCAT's bromine simulation? I am not against the hypothesis, but is it possible to quantify the emissions from SSA and multi-year sea ice? I understand this could not be easy, but currently, the description is very tangled and confusing. Or maybe the author is suggesting blowing snow on multi-year sea ice is more productive than blowing snow on one-year sea ice? The correlation between modelled BrO and contact time with different sea ice types is very low, and their difference (0.17-0.29 vs. 0.03-0.23) is very small. This is not a good support for

the argument in lines 494-495.

A2.8: Thanks for the comment. In the current model's configuration, snow salinity over FYI is based on MOSAiC measurements (Macfarlane et al., 2023), while snow over MYI is assigned half the FYI salinity. As described in A2.5, the sea-ice dataset used in the model can not distinguish between FYI and MYI, and the derived "multi-year" sea ice based on summertime ice is approximate and unreliable. Therefore, the estimated bromine fluxes in p-TOMCAT are not robust or quantitatively meaningful; we are planning to investigate this issue in a more reliable UK Earth System Model.

As shown in Fig 3 and 4, more reliable back-trajectory calculations indicate that air masses spend 2.4 times over MYI than over FYI during BEEs. As a result, MYI accounts for more than half of the cumulative bromine flux, underscoring the important role of MYI in BEEs at Ny-Ålesund.

BrO variability is controlled by multiple factors, including both physical and chemical processes; contact time with the underlying surface is just one of them. Therefore, it is not surprising to see relatively small correlation coefficients between them. Anyway, the data indicate the importance of MYI, which was previously thought to be less important. In the revised manuscript, we have rephrased the sentence as shown below:

"In addition, BrO is positively correlated with both FYI and MYI from March to May, with correlation coefficients between BrO and contact time with MYI (0.17–0.29, $p < 0.0001$) slightly higher than those with FYI (0.03–0.23). These indicate that MYI could play an important role, as FYI does, in determining BEEs at Ny-Ålesund."

Macfarlane, AR, Schneebeli, M, Dadic, R, Tavri, A, Immerz, A, Polashenski, C, Krampe, D, Clem ens-Sewall, D, Wagner, DN, Perovich, DK, Henna-Reetta, H, Raphael, I, Matero, I, Regnery, J, Smith, MM, Nicolaus, M, Jaggi, M, Oggier, M, Webster, MA, Lehning, M, Kolabutin, N, Itkin, P, Naderpour, R, Pirazzini, R, Ha¨mmerle, S, Arndt, S, Fons, S.: A database of snow on sea ice in the central Arctic collected during the MOSAiC expedition. Scientific Data, 10, 398, http:// dx.doi.org/10.1038/s41597-023-02273-1, 2023.

Q2.9: Technical issues:
Line 140: Some information, such as the distance between the Arctic Yellow River Station and Zeppelin Station, should be provided.

A2.9: The horizontal distance between the Arctic Yellow River Station in Ny-Ålesund (78.92° N, 11.93° E) and the Zeppelin Station (78.90° N, 11.88° E) is approximately 2.1 km, based on their geographic coordinates (Platt et al., 2022). This has been added to the manuscript.

"Continuous ozone and GEM measurements have been carried out at Zeppelin Station (78.90° N, 11.88° E; 472 m asl), located approximately 2.1 km from the Arctic Yellow River Station (Platt et al., 2022)."

Platt, S. M., Hov, Ø., Berg, T., Breivik, K., Eckhardt, S., Eleftheriadis, K., Evangeliou, N., Fiebig, M., Fisher, R., Hansen, G., Hansson, H.-C., Heintzenberg, J., Hermansen, O., Heslin-Rees, D., Holmén, K., Hudson, S., Kallenborn, R., Krejci, R., Krognes, T., Larssen, S., Lowry, D., Lund Myhre, C., Lunder, C., Nisbet, E., Nizzetto, P. B., Park, K.-T., Pedersen, C. A., Aspmo Pfaffhuber, K., Röckmann, T., Schmidbauer, N., Solberg, S., Stohl, A., Ström, J., Svendby, T., Tunved, P., Tørnkvist, K., van der Veen, C., Vratolis, S., Yoon, Y. J., Yttri, K. E., Zieger, P., Aas, W., and Tørseth, K.: Atmospheric composition in the European Arctic and 30 years of the Zeppelin Observatory, Ny-Ålesund, Atmos. Chem. Phys., 22, 3321–3369, https://doi.org/10.5194/acp-22-3321-2022, 2022.